HHS Public Access

Author manuscript

Nat Methods. Author manuscript; available in PMC 2022 May 25.

Published in final edited form as:

Nat Methods. 2021 December ; 18(12): 1542–1551. doi:10.1038/s41592-021-01319-9.

Anterograde Transneuronal Tracing and Genetic Control with Engineered Yellow Fever Vaccine YFV-17D

Elizabeth Li[1,*], **Jun Guo**[1,*], **So Jung Oh**[1,*], **Yi Luo**[1], **Heankel Cantu Oliveros**[1], **Wenqin Du**[1], **Rachel Arano**[1], **Yerim Kim**[1], **Yuh-Tarng Chen**[1], **Jennifer Eitson**[2], **Da-Ting Lin**[3], **Ying Li**[1], **Todd Roberts**[1], **John W. Schoggins**[2], **Wei Xu**[1]

[1]Department of Neuroscience, University of Texas Southwestern Medical Center, Dallas, TX, USA.

[2]Department of Microbiology, University of Texas Southwestern Medical Center, Dallas, TX, USA.

[3]Intramural Research Program, National Institute on Drug Abuse, National Institutes of Health, MD, USA.

Abstract

Transneuronal viruses are powerful tools for tracing neuronal circuits or delivering genes to specific neurons in the brain. While there are multiple retrograde viruses, few anterograde viruses are available. Further, available anterograde viruses often have limitations such as retrograde transport, high neuronal toxicity, or weak signals. We developed an anterograde viral system based on a live attenuated vaccine of yellow fever – YFV-17D. Replication-deficient or packaging-deficient mutants of YFV-17D can be reconstituted in the brain, leading to efficient synapse-specific and anterograde-only transneuronal spreading, which can be controlled to achieve either monosynaptic or polysynaptic tracing. Moreover, inducible transient replication of YFV-17D mutant is sufficient to induce permanent transneuronal genetic modifications without causing neuronal toxicity. The engineered YFV-17D systems can be used to express fluorescent markers, sensors or effectors in downstream neurons, thus providing versatile tools for mapping and functionally controlling neuronal circuits.

Introduction

Neuronal circuits are built from multiple types of neurons. These diverse neurons intermingle within the same brain regions and connect to specific neurons distributed locally and/or distally to form complex neuronal circuits, permitting the flow of information and cognition[1]. To study these circuits and to uncover their contributions to brain functions,

Correspondence: Wei.Xu1@UTSouthwestern.edu (W.X.), John.Schoggins@UTSouthwestern.edu (J.S.).
*These authors contributed equally.

Author Contributions

WX initiated, designed and oversaw this study; WX, JS, TR and JG designed the experiments; all authors participated in conducting the experiments, analyzing the results and writing the paper.

Competing interests

The authors declare no competing interests.

it is necessary to delineate how neurons wire together and to control specific neurons. Transneuronal viruses are valuable tools to accomplish these goals. Injected into the brain, these viruses infect neurons, replicate and then cross synapses to reach the connected neurons[2,3]. As self-amplifying tracers, they have been engineered into versatile tools[4–7]. Neurons are polarized cells – receiving information from synapses primarily in the somatodendritic compartment and sending out information through axonal projections. Commonly used transneuronal viruses, such as rabies and herpes simplex viruses (HSV), travel in a retrograde direction – from postsynaptic neurons to presynaptic neurons, and within the individual neurons from axonal terminals back to the somatodendritic compartment[2,3,8]. They are instrumental in revealing inputs to neurons of interest. However, an anterograde virus propagating from presynaptic neurons to postsynaptic neurons will be crucial to revealing synaptic outputs, and to targeting postsynaptic neurons in functional studies.

An ideal anterograde virus is yet to be discovered. Although a few viruses can spread anterogradely, only the H129 strain of HSV1 is predominantly anterograde[9,10]. It has gained broader applications with recent modifications[11,12], but still has a few limitations. It shows retrograde axonal uptake at the injection site and a delayed retrograde transneuronal transport[9,11]. As human pathogen, it is highly toxic to neurons[9,11,13,14]. Besides H129, pseudotyped vesicular stomatitis virus spreads anterogradely, but its efficiency and toxicity have not been extensively examined[15]. Certain serotypes of adeno-associated viruses (AAVs) also spread anterogradely[16,17]; but they show retrograde uptake as well[17,18].

We screened viruses not previously used in neuroscience research and found that a live attenuated vaccine for yellow fever, YFV-17D, spreads between neurons in anterograde direction, albeit with some delayed retrograde transport. Modifications to this virus eliminated retrograde transport and allowed us to develop a series of anterograde-only transneuronal viral vectors for monosynaptic tracing and genetic manipulations.

Results:

Controlled anterograde transneuronal spreading of YFV-17D

YFV-17D is a positive-sense single-stranded RNA virus and encodes one open reading frame whose gene product is post-translationally cleaved into ten proteins (Fig. 1a–b)[19]. Three proteins – C, prM and E – are structural proteins that assemble into viral particles, while the rest – NS1 to NS5 – are not present in virions but are critical to viral replication or egress. YFV-17D encoding the fluorescent protein mVenus (YFV-mVenus) has been described previously[20]. To determine if YFV-17D spreads along brain circuits, we tested YFV-mVenus in a well-characterized pathway, the prefrontal cortex (PFC)-striatum-substantia nigra (SN) pathway (Fig. 1c–d; Extended Data Fig. 1)[21]. We injected YFV-mVenus into the PFC (Fig. 1c). 6 days later, we observed mVenus-positive neurons in the striatum that were surrounded and contacted by axons originating from the PFC (Fig. 1d). At a later time point, we found that YFV-mVenus had continued to travel from the striatum to SN (Extended Data Fig. 1). Similarly, YFV-mVenus spreads along the dentate gyrus-CA3-CA1-subiculum pathway (Extended Data Fig. 2)[22], indicating that YFV-mVenus propagates along neuronal circuits in anterograde direction.

To test if YFV-mVenus also travels in retrograde direction, we injected rAAV2-retro carrying Cre (rAAV2-retro-Cre) into the striatum of tdTomato reporter mice (Ai9 mice)[23] and then injected YFV-mVenus into the same locus 2 weeks later. We fixed the brains after another 6 or 7 days (Fig. 1e–f). We observed tdTomato-positive neurons in the PFC and SN, illustrating that rAAV2-retro retrogradely infected neurons projecting to the striatum (Fig. 1f). We observed mVenus-positive neurons in the SN, which receives projections from the striatum, but not in the PFC, showing that YFV-mVenus moves only in anterograde direction at this time point.

After YFV-mVenus injections, mVenus sensitively reported the presence of viral genes (Extended Data Fig. 3) and was predominantly expressed in neurons (Extended Data Fig. 4–6; Supplementary Fig. 1–2). YFV-17D showed a broad tropism for neurons (Extended Data Fig. 7), and performed similarly in mice of different strains or ages (Supplementary Fig. 3). Mice receiving YFV-mVenus started to show neurological symptoms 16–22 days after the injection (Supplementary Fig. 4–5), which appeared later compared to some other transneuronal viruses, suggesting a lower level of neuronal toxicity[11].

We tested a transcomplementation strategy to control the replication and transport of YFV-mVenus in neuronal circuits by deleting NS1 to generate replication-deficient YFV$^{\Delta NS1}$-mVenus[24]. We constructed the AAV vectors AAV-Syn-NS1 harboring the Synapsin promoter, and AAV-DIO-NS1 encompassing a double-floxed inverted open reading frame, for constitutive or conditional expression of NS1 in neurons, respectively (Fig. 1a–b). We injected AAVDJ-Syn-NS1 into the striatum, and YFV$^{\Delta NS1}$-mVenus into the PFC (Fig. 1g). Red fluorescence appeared in the striatum, indicating expression of NS1 and dTomato. We did not detect mVenus, suggesting that without NS1 being supplied in the PFC, YFV$^{\Delta NS1}$-mVenus was insufficient to replicate and express its genes to a detectable level. When we injected both AAVDJ-Syn-NS1 and YFV$^{\Delta NS1}$-mVenus into the PFC (Fig. 1h), both dTomato and mVenus appeared in the PFC, showing that NS1 expression enabled YFV$^{\Delta NS1}$-mVenus replication and mVenus expression. We did not detect any mVenus-positive neurons in the striatum, suggesting that YFV$^{\Delta NS1}$-mVenus by itself was not sufficient to express mVenus to a detectable level in postsynaptic neurons. When we injected AAVDJ-Syn-NS1 into both the PFC and striatum, and injected YFV$^{\Delta NS1}$-mVenus into the PFC (Fig. 1i), mVenus-positive neurons showed up in both the PFC and the striatum, demonstrating that YFV$^{\Delta NS1}$ replication in the PFC led to transneuronal transport to the striatum, and that NS1 in the striatal neurons enabled YFV$^{\Delta NS1}$ replication and mVenus expression at a detectable level. These results demonstrate that NS1 can control the spreading of YFV$^{\Delta NS1}$. When we injected AAVDJ-NS1 into the PFC and YFV$^{\Delta NS1}$-mVenus into the striatum (Fig. 1j), we did not detect mVenus-positive neurons in the PFC or striatum, suggesting that YFV$^{\Delta NS1}$-mVenus was not subject to retrograde axonal uptake. This result suggests that YFV$^{\Delta NS1}$ may have low affinity to axonal terminals or may not be efficiently transported back to the soma. We also found that AAV-DIO-NS1 could mediate Cre-dependent reconstitution of YFV$^{\Delta NS1}$ (Fig. 1k–l), demonstrating that YFV$^{\Delta NS1}$-mVenus can be targeted to specific neuronal types to trace their connections.

To test if YFV was exclusively anterograde, we injected AAVDJ-NS1 into both the PFC and striatum, and 2 weeks later injected YFV$^{\Delta NS1}$-mVenus into the striatum (Extended Data Fig.

8). After another 6 or 7 days, we did not detect any mVenus-positive neurons in the PFC, consistent with anterograde-only transport of YFV-mVenus at this time point. However, 12 days after injection, mVenus-positive neurons appeared in the PFC, suggesting a temporally delayed retrograde transport of $YFV^{\Delta NS1}$-mVenus.

Anterograde-only tracing by inducible replication of $YFV^{\Delta NS1}$

To eliminate the delayed retrograde transport, we hypothesized that in the early stage of infection a limited number of viral proteins and virions are produced and selectively carried by the anterograde cellular transport machinery. Over time, the virus continues to replicate and eventually exceeds the capacity of selective anterograde delivery. Thus, anterograde-only transport may be achieved by limiting viral replication to a low level or short period.

We therefore constructed an inducible system to control $YFV^{\Delta NS1}$ replication (Fig. 2a). In this system, we used either AAV-rtTA or AAV-tTA to make NS1 expression dependent on the presence or absence of doxycycline (Dox), respectively. NS1 expression can be controlled by adjusting the dosage, frequency and timing of Dox. We made two versions of AAV-TRE-NS1: AAV-TRE-NS1/dTomato encodes a fluorescent protein; AAV-TRE-NS1/NF does not. To validate this system, we injected into the PFC different combinations of AAVs, and 2 weeks later, $YFV^{\Delta NS1}$-mVenus (Fig. 2b). We quantified viral genomic copies in PFC tissues. AAVDJ-Syn-NS1, or AAVDJ-rtTA plus AAVDJ-TRE-NS1 in the presence of Dox, or AAVDJ-tTA plus AAVDJ-TRE-NS1 in the absence of Dox, increased YFV genomic copies by more than 10,000 folds from the background level. Histology analysis showed similar results (Supplementary Fig. 6). The results demonstrate that rtTA or tTA and Dox can control the replication of $YFV^{\Delta NS1}$-mVenus.

To test if we could achieve anterograde-only tracing with this system, we injected AAVDJ-rtTA and AAVDJ-TRE-NS1/dTomato into both the PFC and striatum, and then injected $YFV^{\Delta NS1}$-mVenus in either the PFC or striatum (Fig. 2c–e). We injected Dox at different frequencies to adjust the level and timing of NS1 expression (Fig. 2c and Supplementary Fig. 7). We perfused mice 12 days after $YFV^{\Delta NS1}$-mVenus injection to match the time when $YFV^{\Delta NS1}$-mVenus showed retrograde transport with the help of AAV-NS1 (Extended Data Fig. 8). When we followed a typical protocol (Fig. 2c) and injected $YFV^{\Delta NS1}$-mVenus into the PFC, mVenus-positive neurons appeared in both the PFC and striatum, indicating anterograde transport of $YFV^{\Delta NS1}$-mVenus (Fig. 2d). By contrast, when we injected $YFV^{\Delta NS1}$-mVenus into the striatum, we observed mVenus-positive neurons only in the striatum but not PFC, suggesting no retrograde transport of $YFV^{\Delta NS1}$-mVenus (Fig. 2e). These data demonstrate that by temporally restricting NS1 expression we can achieve anterograde-only transport of $YFV^{\Delta NS1}$-mVenus.

We quantified the anterogradely labeled neurons in the striatum by using either concentrated (titer: 9.60×10^{10} genome copies/ml) or 5–10 fold diluted $YFV^{\Delta NS1}$-mVenus (Fig. 2f). We found that the number of traced neurons in the striatum depends on the amount of $YFV^{\Delta NS1}$-mVenus injected into the PFC, which may reflect the number of starter neurons in which tracing originated.

Dual fluorescence tracing of parallel circuits

To uncover how neural circuits diverge or converge, we generated YFV$^{\Delta NS1}$-mCherry. We then traced the pathways from two cortical regions—the PFC and motor cortex (Mo)—to the midbrain with YFV$^{\Delta NS1}$-mVenus and YFV$^{\Delta NS1}$-mCherry, respectively, with NS1 provided in the PFC, Mo and midbrain (Fig. 3a–c). mVenus- or mCherry- positive axons from the PFC or Mo, respectively, passed the dorsal striatum and then diverged to different nuclei in the midbrain.

We then tested if the YFV$^{\Delta NS1}$ system could trace polysynaptic pathways as well. We provided NS1 in the striatum in addition to PFC, Mo and midbrain (Fig. 3d–f; Supplementary Fig. 8). In the striatum, we observed mVenus- or mCherry- positive neurons, with mVenus concentrated in the dorsomedial and mCherry in the dorsolateral striatum. In the midbrain, mVenus-positive neurons were densely distributed in the SN and ventral tegmental area (VTA), showing that more SN and VTA neurons receive indirect PFC innervation via the striatum than those receiving direct PFC innervation. mCherry-positive neurons were concentrated in the red nucleus (RN). We also examined the projection from the PFC and primary somatosensory cortex (SSp) to the midbrain (Supplementary Fig. 9). Both experiments demonstrate largely separate cortex-striatum-midbrain pathways.

Transneuronal genetic control by YFV$^{\Delta NS1}$-Cre

We created YFV$^{\Delta NS1}$-Cre to functionally manipulate postsynaptic neurons. YFV$^{\Delta NS1}$-Cre can be induced to replicate transiently and make permanent genetic modifications in postsynaptic neurons. The transient viral replication minimizes neuronal toxicity caused by unrestricted viral replication (Fig. 4a). We injected AAVs for inducible expression of NS1 into the PFC and striatum; and we injected AAV9-DIO-jGCaMP7f into the striatum to mediate Cre-dependent expression of jGCaMP7f[25](Fig. 4b). We injected YFV$^{\Delta NS1}$-Cre into the PFC and fixed the brains 15 or 30 days after YFV$^{\Delta NS1}$-Cre injections. We found jGCaMP7f-positive neurons in the striatum (Fig. 4c), showing that YFV$^{\Delta NS1}$-Cre can modify genes in postsynaptic neurons. The density of jGCaMP7f-positive neurons did not change from 15 to 30 days (Fig. 4d), suggesting low neuronal toxicity of this system.

To test if YFV$^{\Delta NS1}$-Cre from the PFC was sufficient to turn on reporters in downstream regions without replication, we omitted the AAVs expressing NS1 in striatal injections (Extended Data Fig. 9). YFV$^{\Delta NS1}$-Cre turned on jGCaMP7f expression, albeit with low efficiency.

We conducted electrophysiological recordings to verify synaptic connections between the PFC starter neurons and the traced striatal neurons (Fig.4e–g). In all of the jGCaMP7f-positive striatal cells recorded, optogenetic stimulation of the axonal terminals originating from PFC elicited postsynaptic currents. In 11 of the 12 jGCaMP7f-positive cells the synaptic latencies were in the range of 0.3 to 2.2 ms, suggesting monosynaptic connections[26]. No synaptic responses were elicited in 4 of the 12 jGCaMP7f-negative cells. In the remaining 8 jGCaMP7f-negative cells optostimulation elicited synaptic responses with low amplitudes and longer synaptic delays, suggesting that they were not monosynaptic responses (Fig. 4g). The basic membrane properties and spontaneous synaptic activities of

the recorded jGCaMP7f-positive or -negative cells were similar (Supplementary Fig. 10), suggesting that the labeled cells were healthy.

To test if YFV$^{\Delta NS1}$-Cre could help to monitor long-term neuronal activity (Fig. 4h–j), we injected YFV$^{\Delta NS1}$-Cre into the PFC to turn on the expression of jGCaMP7f in the striatum and conducted calcium imaging in freely moving mice with a miniaturized microscope through a lens implanted in the striatum (Fig. 4h)[27]. We detected robust neuronal calcium signals (Fig. 4i). Most of the neurons identified at 6 weeks were detected again at 7 weeks (Fig. 4j, and Supplementary videos 1 and 2), indicating that YFV$^{\Delta NS1}$-Cre can mediate anterograde transneuronal genetic manipulations; and the transient activation of YFV$^{\Delta NS1}$-Cre can lead to long-term expression of reporter genes.

Mapping monosynaptic projectomes with YFV$^{\Delta CME}$

To trace the whole-brain projection patterns of defined neurons (projectomes), we constructed the packaging-deficient YFV$^{\Delta CME}$ by removing the structural proteins C, prM and E (Fig. 5a). To infect cells, YFV$^{\Delta CME}$ needs the structural proteins (Supplementary Fig. 11), which are provided only in starter neurons, for transneuronal spreading. Therefore, this YFV variant spreads only monosynaptically from the starter neurons. Since viral genes do not need to be provided in post-synaptic neurons, the projections in the whole brain can be traced.

We then tested this system *in vivo* and compared it to AAV-SynaptoTAG2 (Fig. 5b, an updated version of the AAV-SynaptoTAG[28]), which expresses tdTomato to reveal neuronal somas and axons, and EGFP fused to Synaptobrevin-2 to track synaptic terminals. After injecting AAVDJ-SynaptoTAG2 into the PFC, we observed EGFP-positive synaptic terminals in the brain regions downstream of the PFC (Fig. 5c). To test YFV$^{\Delta CME}$, we injected the AAVs to express C-prM-E (AAVDJ-TRE-C-prM-E-NS1 and AAVDJ-tTA) into the PFC and fed mice with a Dox-containing diet. Two weeks later we injected YFV$^{\Delta CME}$-mVenus into the PFC. Another 7 or 8 days later, we perfused the mice. We detected mVenus-positive neurons in the brain regions innervated by PFC neurons (Fig. 5d–g; Supplementary Fig. 12), similar to the connections detected with SynaptoTAG2. The densities of mVenus-positive cells positively correlated with the intensity of SynaptoTAG2 labeling (Supplementary Fig. 13). We also tested this system with other brain circuits, such as the projections from pontine nuclei (Extended Fig. 10), SN and VTA area (Supplementary Fig. 14) or motor cortex (Supplementary Fig. 15).

YFV$^{\Delta CME}$ can replicate in the infected neurons. This unrestricted replication eventually leads to cell toxicity and neuronal death (Supplementary Fig. 16). Therefore, neuronal projection patterns should be analyzed shortly after injection (in 7–9 days).

Monosynaptic transneuronal genetic control with YFV$^{\Delta CMENS1}$

To combine the advantages of YFV$^{\Delta NS1}$-Cre (minimal neuronal toxicity) and YFV$^{\Delta CME}$ (monosynaptic spreading), we constructed YFV$^{\Delta CMENS1}$-Cre by removing C-prM-E and NS1 (Fig. 6a). When both C-prM-E and NS1 are expressed in starter cells, YFV$^{\Delta CMENS1}$-Cre can replicate in the starter cells and propagate to postsynaptic neurons. NS1 provided in the postsynaptic neurons enables the replication of YFV genome to enhance the expression

of Cre, but does not allow YFV to spread further (Fig. 6b). Tested in the PFC-striatum pathway, YFV$^{\Delta CMENS1}$-Cre induced genetic modifications transneuronally to turn on the expression of reporters in postsynaptic neurons in the striatum (Fig. 6c–f). The density of the traced striatal neurons did not change from 15 to 30 days, suggesting that YFV$^{\Delta CMENS1}$-Cre did not cause neuronal loss (Fig. 6g).

Discussion

Transneuronal viruses are useful tools because they can both carry various genes across synapses and self-amplify the signal. Here we identified YFV-17D as a primarily anterograde transneuronal virus and used two transcomplementation strategies to improve its performance. Each of the strategies has its own advantages and limitations and can be chosen for different applications. Deletion of the NS1 gene in YFV$^{\Delta NS1}$ targeted the viral replication process; and we achieved anterograde-only tracing and minimized neuronal toxicity with this strategy. Since NS1 is needed in postsynaptic neurons for efficient tracing or genetic manipulation, this system is ideal for studying the interactions between two chosen brain regions or two groups of neurons. Deletion of the genes for structural proteins in YFV$^{\Delta CME}$ leveraged the assembly of viral particles. This system is ideal for mapping monosynaptic projections at the whole-brain scale. However, neuronal toxicity may limit its applications in functional analyses. We further combined these two strategies by generating YFV$^{\Delta CMENS1}$-Cre to achieve monosynaptic transneuronal genetic modifications.

A few lines of evidence support the synapse specificity of YFV-17D in transneuronal transport. Firstly, YFV-17D traveled along well-characterized pathways including the PFC-striatum-midbrain[21] and the DG-CA3-CA1-subiculum pathways[29]. Secondly, it propagated to synaptically connected neurons while sparing non-connected neurons in the same regions. Thirdly, it did not infect neurons along the route of axons from infected neurons, showing that the virus does not spread between cells just based on proximity. In addition, electrophysiological recording in traced neurons confirms functional synaptic connections. The synaptic specificity enables the engineered YFV-17D systems to target specific postsynaptic neurons for selective observation or functional manipulation.

To elucidate brain functional organization, control over specific postsynaptic neurons is imperative. Recently, retrograde transneuronal genetic manipulations have been substantially improved with the reduction of neurotoxicity of the rabies virus[30–32]. Yet an anterograde-only transneuronal virus for genetic control was still needed. Non-viral approaches for anterograde transneuronal genetic manipulations have been described[33–37]. However, their low efficiency in mammals or lack of direction selectivity limited their applications. The YFV$^{\Delta NS1}$ (and YFV$^{\Delta CMENS1}$) system has advantages in this respect. Firstly, when NS1 is provided, YFV$^{\Delta NS1}$ can replicate and amplify the expression of Cre or other genetic tools in postsynaptic neurons. Secondly, genetic manipulation can be induced in both monosynaptic and polysynaptic targets. Thirdly, the inducible transient replication of YFV$^{\Delta NS1}$ eliminates concerns about neuronal toxicity caused by viral replication.

In summary, the engineered YFV-17D systems are valuable viral vectors for studying brain circuits. They have several advantages (Supplementary Table 1) and are convenient to

construct and package. YFV-17D has been used in humans for over 80 years[38]. Building on this anterograde tracer, we expect the engineered YFV-17D will be developed into tools for broader applications in research or even in clinical treatments of neuropsychiatric disorders.

Methods:

Mice:

2-month-old male C57BL/6J mice (UT Southwestern breeding core or the Jackson Laboratory) were used in all of the experiments except for experiments in Fig.1e–f and Supplementary Fig. 3. 2-month-old male BALB/c mice and 6-month-old female C57BL/6J mice (the Jackson Laboratory) were used for experiments in Supplementary Fig. 3. 2-month-old male tdTomato reporter mice, Ai9 mice (the Jackson Laboratory, stock No. 007909) were used for the experiment reported in Fig.1e–f. The mice were group-housed on a 12 hr light/12 hr dark cycle with ad libitum access to food and water. Mice were randomly assigned to experimental groups. Animal work was approved and conducted under the oversight of the UT Southwestern Institutional Animal Care and Use Committee and complied with Guide for the Care and Use of Laboratory Animals by National Research Council.

Cell culture:

293T cells, grown in Dulbecco's Modified Eagle's Medium (DMEM) containing 10% FBS, were used to generate AAVDJ. BHK cells (ATCC CCL-10) or human *STAT1*$^{-/-}$ fibroblasts (a gift from Dr. J-L. Casanova at Rockefeller University) were used to generate YFV-17D and its mutants.

Viral vector construction:

Genes were cloned into AAV *cis*-plasmid (AAV2 serotype). In AAV-tTA or AAV-rtTA, the following components were arranged sequentially downstream of left inverted terminal repeats (ITR): synapsin promoter, tTA or rtTA, posttranscriptional regulatory element (WPRE), hGH poly A sequence, and the right ITR. In AAV-NS, the following components were arranged sequentially downstream of left-ITR: synapsin promoter, NS1, P2A, dTomato with SV40 nuclear localization signal or sequence (NLS), WPRE, hGH poly A sequence, and the right ITR. In AAV-DIO-NS1, the following components were arranged sequentially downstream of left-ITR: synapsin promoter, LoxP site and Lox2272 site, inverted open reading frame containing the coding sequences of NS1, P2A and NLS-dTomato, LoxP site, Lox2272 site, WPRE, hGH poly A sequence, and the right ITR. In AAV-TRE-NS1/dTomato, the following components were arranged sequentially downstream of left-ITR: the coding sequence of dTomato (with nuclear localization signal), bidirectional TRE promoter, coding sequences of NS1, WPRE, hGH poly A sequence, and the right ITR. The dTomato in AAV-TRE-NS1/dTomato was removed to generate AAV-TRE-NS1/NF. AAV-TRE-CMENS1 was made by replacing the NS1 in AAV-TRE-NS1/NF with the coding sequence of C-prM-E-NS1 (from methionine 1 to alanine 1130 of YFV coding sequence).

The infectious clone encoding YFV-mVenus, YF17D-5′C25Venus2AUbi, was constructed previously by in-frame insertion of a coding sequence, which consists of the

first 25 amino acids of the YFV polyprotein, mVenus, the foot-and-mouth disease virus (FMDV) 2A peptide, and an ubiquitin (Ubi) monomer, at the N-terminus of the YFV-17D polyprotein in a PCC1 vector[39]. The infectious clone for YFV$^{\Delta NS1}$-mVenus, YF17D-5′C25Venus2AUbiΔNS1, was constructed as follows. The parental YF17D-5′C25Venus2AUbi plasmid was digested with NsiI and MluI, and the NS1-containing fragment was subcloned into pSL1180 to generate pSL1180.YFV17D-NM. This plasmid was digested with SacI and MluI to remove sequences encoding NS1 amino acids 14 −165. An oligo encoding a flexible GSRSG linker was ligated into the digested vector to generate pSL1180.YFV17D-NMΔNS1. The NsiI-MluI fragment bearing the truncated NS1 sequence was subcloned back into the parental infectious clone to generate YF17D-5′C25Venus2AUbiΔNS1. The coding sequence of mVenus in YFV$^{\Delta NS1}$-mVenus was then replaced with the coding sequences of mCherry or Cre to generate YFV$^{\Delta NS1}$-mCherry or YFV$^{\Delta NS1}$-Cre, respectively. YFV$^{\Delta CME}$-mVenus was constructed from parental YF17D-5′C25Venus2AUbi by removing the coding sequence of C-prM-E (from serine 22 to Arginine 754 of YFV coding sequence). YFV$^{\Delta NS1}$-mCherry was made by replacing mVenus in YFV$^{\Delta NS1}$-mVenus with mCherry. YFV$^{\Delta CMENS1}$-Cre was made from YFV$^{\Delta CME}$-mVenus by replacing NS1 amino acids 14 −165 with a GSRSG linker as described for YFV$^{\Delta NS1}$-mVenus, and replacing mVenus with Cre. The sequences of the plasmids were confirmed with restriction digests and sequencing.

Virus production:

All AAVs except rAAV2-retro-cre and AAV-DIO-jGCaMP7f were packaged into AAVDJ serotype. AAV2-retro-cre was packaged with rAAV2-retro capsid genes (rAAV2-retro helper plasmid[23]). Virus was prepared as described[40]. Briefly, AAV vectors were co-transfected with pHelper and pRC-DJ or rAAV2-retro helper into AAV-293 cells. Cells were collected 72 hr later, lysed, and loaded onto an iodixanol gradient for centrifugation at 400,000 g for 2 hr. The fraction with 40% iodixanol of the gradient was collected, washed, and concentrated with 100,000 MWCO tube filter. The genomic titer of virus was measured with quantitative real-time PCR. The titers of AAVs used for stereotaxic injection were in the range of 0.5–2 × 10^{13} genome copies/ml. AAV-DIO-jGCaMP7f packaged in AAV9 capsid (titer: 2.7×10^{13}) was purchased from Addgene.

To generate YFV-17D stocks, plasmids were linearized with XhoI digestion and transcribed with an SP6 in vitro transcription kit (mMESSAGE mMACHINE Kit, Ambion). The quality of transcribed RNAs were confirmed with bioanalyzer 2100. The full-length in vitro transcribed YFV RNAs were then electroporated into human *STAT1*$^{-/-}$ fibroblasts (a gift from Dr. J-L. Casanova) or BHK cells (ATCC, Cat# CCL-10). The fibroblasts were grown in RPMI containing 10% fetal bovine serum (FBS) and nonessential amino acids. BHK cells were cultured with DMEM plus 10% FBS. Virus containing supernatants were concentrated in 100K Amicon Ultra Centrifugal Filters (Millipore), aliquoted and stored at −80C. Viral stocks were titered by qRT-PCR. To generate YFV$^{\Delta NS1}$, YFV$^{\Delta CME}$, or YFV$^{\Delta CMENS1}$ virus, a complementation cell line was generated by transducing STAT1−/− fibroblasts or BHK cells with lentiviral vectors expressing NS1 or C-prM-E-NS1. In vitro transcribed viral RNAs, generated from linearized plasmids encoding YFV$^{\Delta NS1}$, YFV$^{\Delta CME}$, or YFV$^{\Delta CMENS1}$as described above, was electroporated into the STAT1−/− fibroblasts (NS1)

or transfected into BHK cells with TransIT-mRNA Transfection Kit (Mirus Bio, Cat.# MIR 2225). As described above, virus containing supernatant was concentrated, aliquotted, stored at −80C, and titered by qRT-PCR. The titers of the YFV17D and mutants used were YFV-mVenus, 1.01×10^{11}; $YFV^{\Delta NS1}$-mVenus, 1.57×10^{11}; $YFV^{\Delta NS1}$-mCherry, 1.81×10^{11}; $YFV^{\Delta NS1}$-Cre, 9.60×10^{10}; $YFV^{\Delta CME}$-mVenus, 5.46×10^{11}; $YFV^{\Delta CMENS1}$-Cre, 3.71×10^{11} genome copies/ml.

Stereotaxic viral injection and Dox administration:

Mice were anesthetized with tribromoethanol (125–250 mg/kg) or isoflurane inhalation (1.5–2%). Viral solution was injected with a glass pipette at a flow rate of 0.10 μl/min. After the completion of injection, the glass pipette was left in place for 5 min before being retrieved slowly. We unilaterally injected between 0.25 – 0.5 μl of viral solution at each injection site unless stated otherwise. In most of the injections we moved the injection pipette in the vertical direction. In the striatal injections in Fig. 3, to avoid the impact of virus leaking into injection track, we injected AAVs at 45 degree and injected $YFV^{\Delta NS1}$-mVenus vertically. The coordinates for each of the injection sites on the anterior-posterior direction from the bregma (AP), medial-lateral direction from the midline (ML), and the dorsal-ventral direction from the dura (DV) are as follows (In the AP direction, "+" denotes anterior to the bregma and "-" denotes posterior to bregma.): PFC (+1.25, 0.30, 1.25); DG (−2.00, 1.25, 2.20); CA1 (−1.95, 1.35, 1.20); SN (−3.15, 1.15, 5.50); Mo (+0.45, 1.50, 0.80); SSp (+0.45, 3.50, 1.00); striatum (vertical) (+0.55, 1.65, 3.00); striatum (45 degree) (+0.50, 3.50, 2.40). Dox was administrated either through intraperitoneal injections (50mg/kg body weight, dissolved in pre-warmed saline) or through feeding with Dox diet (containing doxycycline hyclate, 625 mg/kg diet).

Histology and microscopy:

Mouse brains were fixed by transcardial perfusion of 10 ml of phosphate-buffered saline (PBS) followed by 40 ml of 4% paraformaldehyde (PFA) in PBS. The brains were postfixed overnight in 4% PFA at 4°C and were then incubated in 30% sucrose for at least 24 hours. Brains were embedded in Tissue-Tek OCT compound, frozen on dry ice, and then sectioned to a thickness of 40-μm with cryostat. For regular histological analysis, free-floating sections were washed in PBS for 3 times, stained with DAPI (1μg/ml, diluted in PBS) and mounted on glass slides. The whole-mount brain sections were scanned with Zeiss AxioscanZ1 digital slide scanner with a 10X objective. The high-resolution images were taken with ZEISS LSM 880 with Airyscan confocal microscope. For immunohistochemistry, the brain sections were washed in PBS for 3 times and permeabilized in 2% triton X-100 in PBS for 2 hours. The sections were then incubated for 2 hours in PBS containing 10% horse serum, 0.2% bovine serum albumin (BSA) and 0.5% triton X-100, followed by overnight incubation in primary antibodies diluted in PBS containing 1% horse serum (HS) and 0.2% bovine serum albumin (BSA). The primary antibodies used in this study and their dilutions are as the following: NeuN antibody (clone A60), Sigma MAB377, 1:1000; opioid receptor-Mu (MOR) antibody, Immunostar 24216, 1:500; PCP4 antibody, Sigma HPA005792, 1:1000; tyrosine hydroxylase antibody, Millipore AB152, 1:1000; YFV NS1 antibody, Aviva Systems Biology OAEF00516, 1:1000; YFV protein E antibody, Abbexa abx411683, 1:2000; ALDH1L1 antibody (Clone: UMAB43), Origene UM570039, 1:200;

TMEM119 antibody, AbCam ab209064, 1:500; NG2 antibody, Sigma/Millipore AB5320, 1:500; Olig2 antibody (clone 211F1.1), Sigma/Millipore MABN50, 1:200. After 3 washes in PBS, the sections were then incubated in the secondry antibodies for 2 hours, washed again and then mounted onto glass slides. The secondary antibodies used in this study and their dilutions were Alexa Fluor 594-conjugated goat anti-mouse or goat anti-rabbit IgG (Thermo Fisher) 1:500.

Brain slice electrophysiology:

We prepared coronal brain slices of the striatum (300 μm in thickness) with a Leica VT1200 vibratome. Slicing was made in ice-cold cutting solution, which contained (in mM): 1.2 NaH_2PO_4, 26 $NaHCO_3$, 2.5 KCl, 0.5 $CaCl_2$, 7 $MgCl_2$, 11 D-glucose, 5 Na-ascorbate, 3 Na-pyruvate and 220 sucrose. The slices were recovered by incubation in artificial cerebrospinal fluid (ACSF) containing (in mM): 124 NaCl, 1.2 NaH_2PO_4, 26 $NaHCO_3$, 5 KCl, 1.3 $MgCl_2$, 2.5 $CaCl_2$ and 11 D-glucose at 32 °C for 30 min and at room temperature for more than 1 hour. The pH value and osmolality of the cutting solution and ACSF were adjusted to pH 7.3–7.4 and 290–300 mOsm. The solutions were aerated with 95% O_2/5% CO_2. The slices were perfused with oxygenated ACSF in a recording chamber (~1 ml/min) at 26–28 °C. Whole-cell patch clamp recording was performed with recording pipettes (2.5–4 MΩ) filled with internal solution containing (in mM): 0.3 Na-GTP, 10 Na_2-phosphocreatine, 20 KCl, 125 K-gluconate, 4 Mg-ATP, 0.5 EGTA, 10 HEPES, adjusted to pH 7.3–7.4 and 310 mOsm. Data were collected with pCLAMP and analyzed with clampfit (Molecular Devices). For optogenetic stimulation of axonal terminals, 2-ms blue light (473 nm) pulses were delivered by LED coupled with a 40X water objective.

RNA extraction and quantification:

The mouse brains were quickly removed after euthanasia and cut into 1-mm slices in a pre-chilled brain matrix. PFC tissues were dissected out and homogenized for RNA extraction with QIAamp Viral RNA Mini Kit following the manufacturer's protocol. The concentrations of the total RNA from each of the mice were determined with NanoDrop 2000 spectrophotometer. Equal amounts of total RNA were loaded for real-time PCR on Applied Biosystems 7500 Fast Real-Time PCR System with Taqman assay to quantify the genomic copies of YFV. The Taqman assay consisted of a forward primer (GCCTCCCACATCCATTTAGT), a reverse primer (CAGGTCAGCATCCACAGAATA), and a probe (CCGAACGCTGATTGGACAGGAGAA). A serial dilution of a linearized plasmid containing the coding sequence of YFV was used to generate a standard curve for the real-time PCR assay.

Implantation of GRIN lenses and calcium imaging of freely moving mice:

Mice were anesthetized and injected with a combination of viral solutions (AAVDJ-rtTA / AAVDJ-TRE-NS1-dTomato mixed at a 1:1 ratio) at the PFC and the striatum at the coordinates indicated above. An additional AAV-DIO-jGCaMP7f was injected into the striatum. 2 weeks later, the mice were anesthetized and injected with $YFV^{\Delta NS1}$-Cre into the PFC, immediately followed by the implantation of a GRIN lens of 0.5-mm diameter into the striatum (coordinates: AP +0.55, ML 1.65, DV 2.10). The lens was then fixed onto the skull with Metabond quick adhesive cement system followed by regular dental cement. A

plastic tube was placed around the lens to protect the part of GRIN lens exposed on the skull. 2 weeks later, the plastic protection tube was removed and a metal holder was fixed onto the skull with dental cement. The metal holder was used to connect the GRIN lens to a minimized microscope to image calcium signal during behavioral tests[41]. The images were motion correction with NoRMCorre[42]. The calcium signals were then extracted and analyzed with the extended CNMF for microendoscopic data (CNMF-E) approach[43].

Quantification and Statistical Analysis

Data are presented as scatter and mean ± standard error of the mean (SEM). The experiments were repeated for the number of times as shown in the legends. Statistical difference was analyzed with two-tailed Mann-Whitney test. $P < 0.05$ was considered statistically significant.

Extended Data

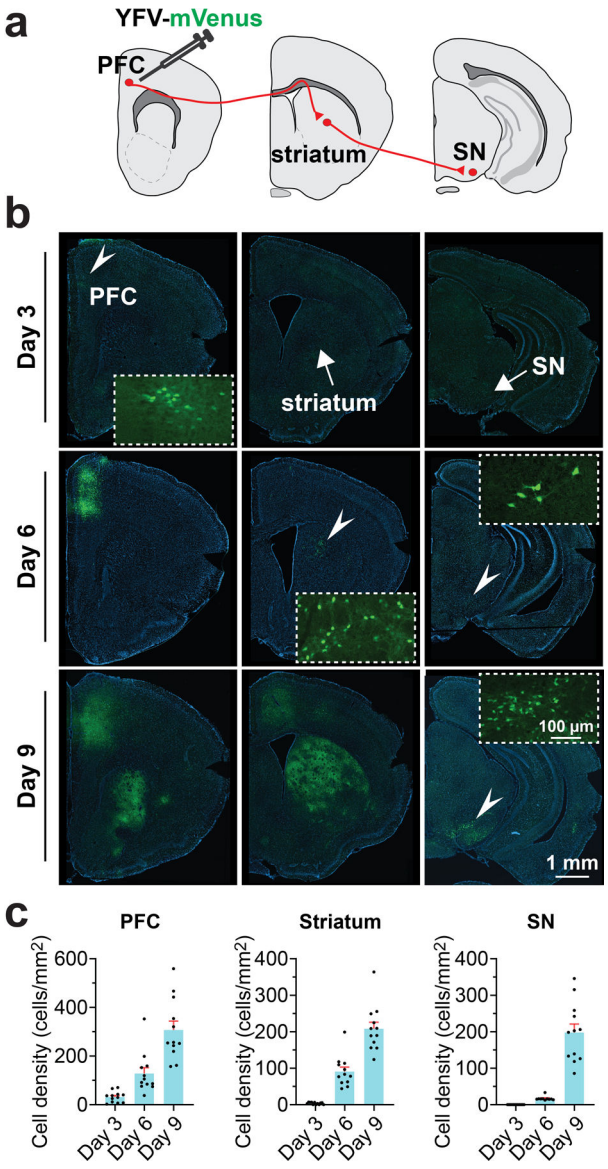

Extended Data Figure 1.

(**a**) Schematics showing the PFC-striatum-SN pathway. (**b**) Expression of mVenus after injection of YFV-mVenus into the PFC. Brains were collected 3, 6 or 9 days after injection. All images are tile scans of brain sections. The blue color is counterstaining with DAPI. (**c**) Quantification of images in **b**: Density of mVenus-positive neurons in each brain region on day 3, 6, and 9. The bars are mean±SEM, n=10–12 sections from 3 mice for each brain region.

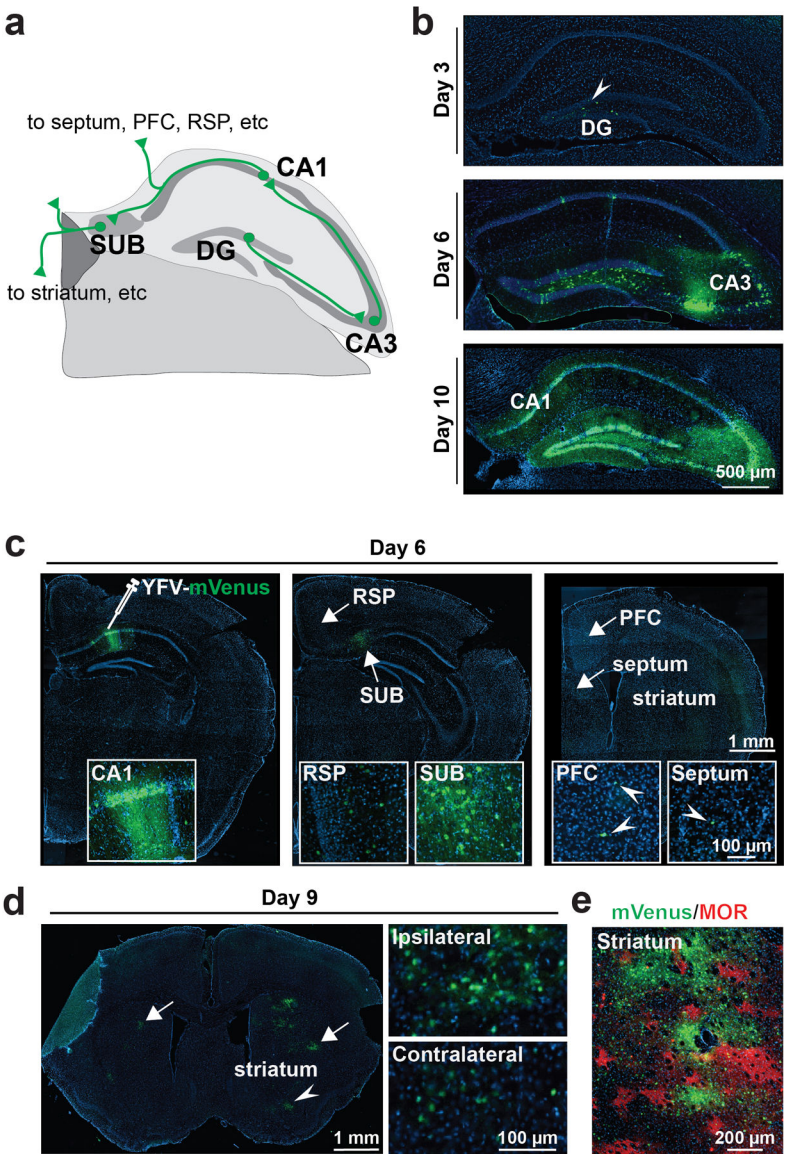

Extended Data Figure 2.

(**a**)The dentate gyrus (DG)-CA3-CA1-subiculum (SUB)-striatum pathway. (**b**) Expression of mVenus after injection of YFV-mVenus into the DG. Brains were collected 3, 6 or 10 days after injection. (**c**-**e**) YFV-mVenus spread from the CA1 to SUB and dorsal striatum along polysynaptic pathways. mVenus expression after YFV-mVenus injection into dorsal CA1. Brains were collected 6 (**c**), 9 (**d**) or 11 (**e**) days after injection. (**e**) Images of brain sections containing the striatum from a mouse 11 days after YFV-mVenus injection at dorsal CA1 that were immunostained with MOR, a marker for striosomes. The experiments were repeated 3 times with similar results. All images are tile scans of brain sections. The blue color is counterstaining with DAPI.

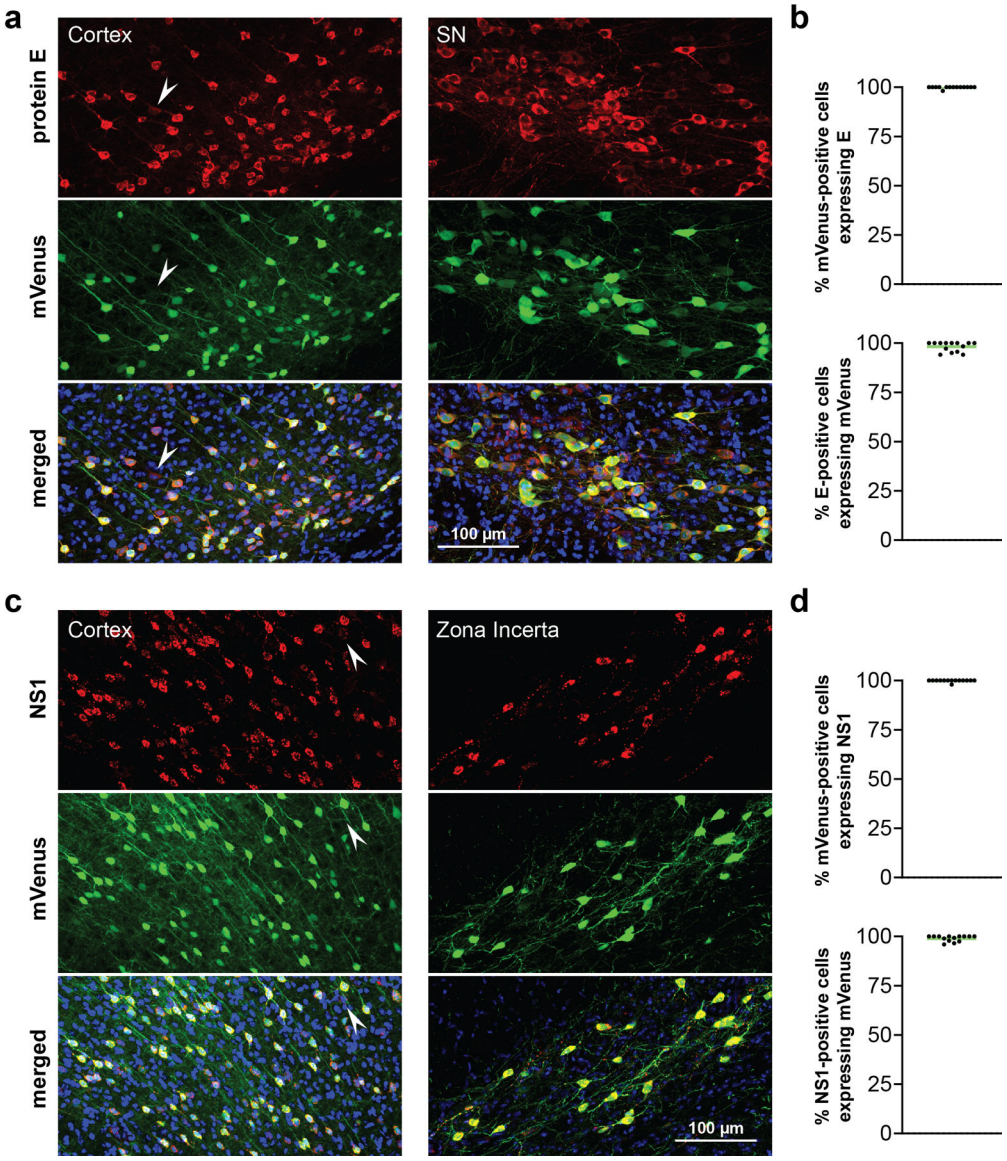

Extended Data Figure 3.

(**a**) Images of brain sections from mice infected with YFV-mVenus that were immunostained with antibody for YFV protein E. The green fluorescence was from native mVenus without immunostaining. The arrowheads indicate cells positive for E but not mVenus. (**b**) Quantification of mVenus-positive cells expressing E, and E-positive cells expressing mVenus. (**c**) Images of brain sections from mice infected with YFV-mVenus that were immunostained with antibody for NS1. The arrowheads indicate cells positive for NS1 but not mVenus. (**d**) Quantification of mVenus-positive cells expressing NS1, or NS1-positive cells expressing mVenus. n=14 brain sections from 3 mice for “E” and n=14 brain sections from 4 mice for “NS1”. All images are tile scans of brain sections. The blue color is counterstaining with DAPI.

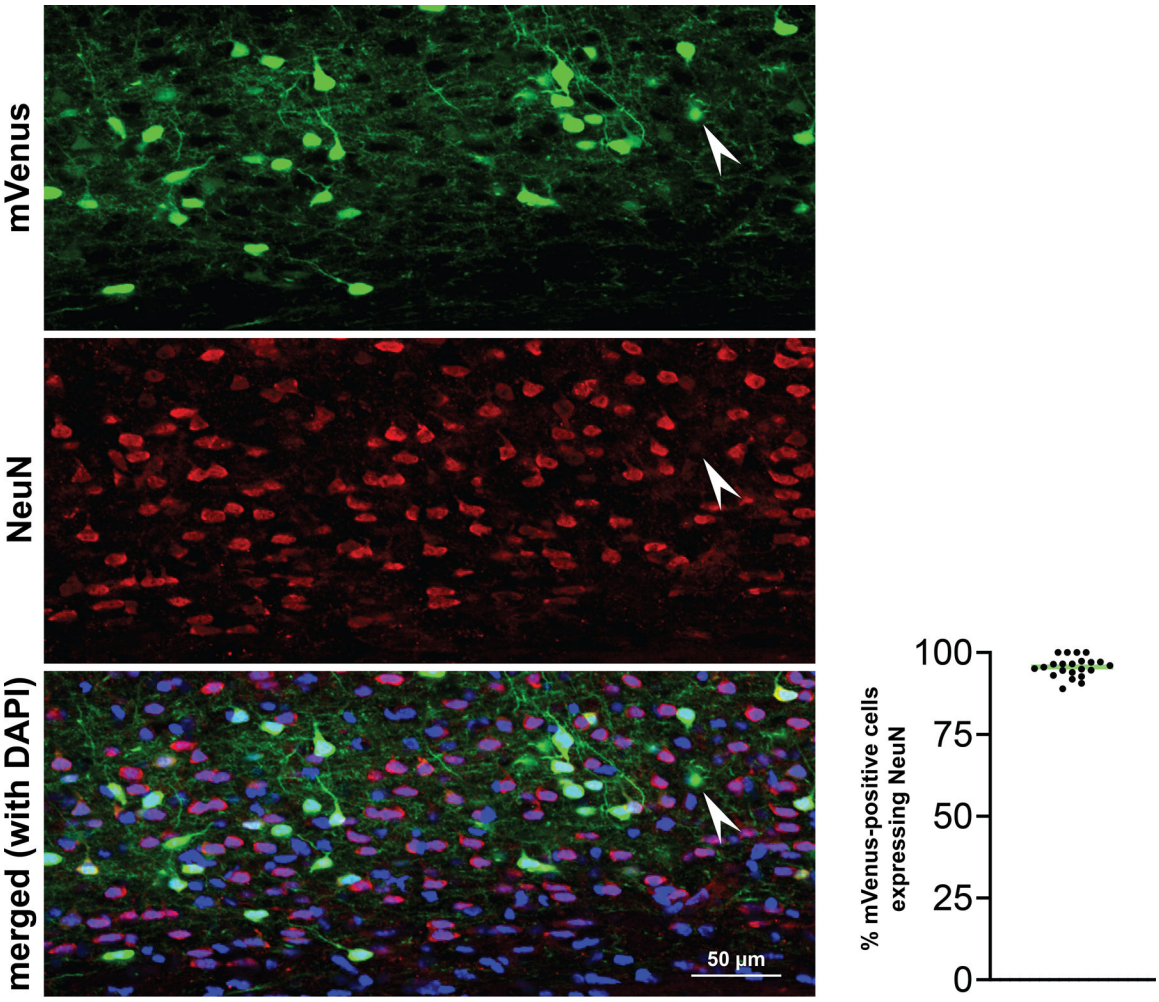

Extended Data Figure 4.

Expression of the neuronal marker NeuN in brain sections from mice infected with YFV-mVenus. The green fluorescence was from native mVenus without immunostaining. The arrowheads indicate a non-neuronal cell expressing mVenus. n=22 brain sections from 3 mice. The images are tile scans of brain sections. The blue color is counterstaining with DAPI.

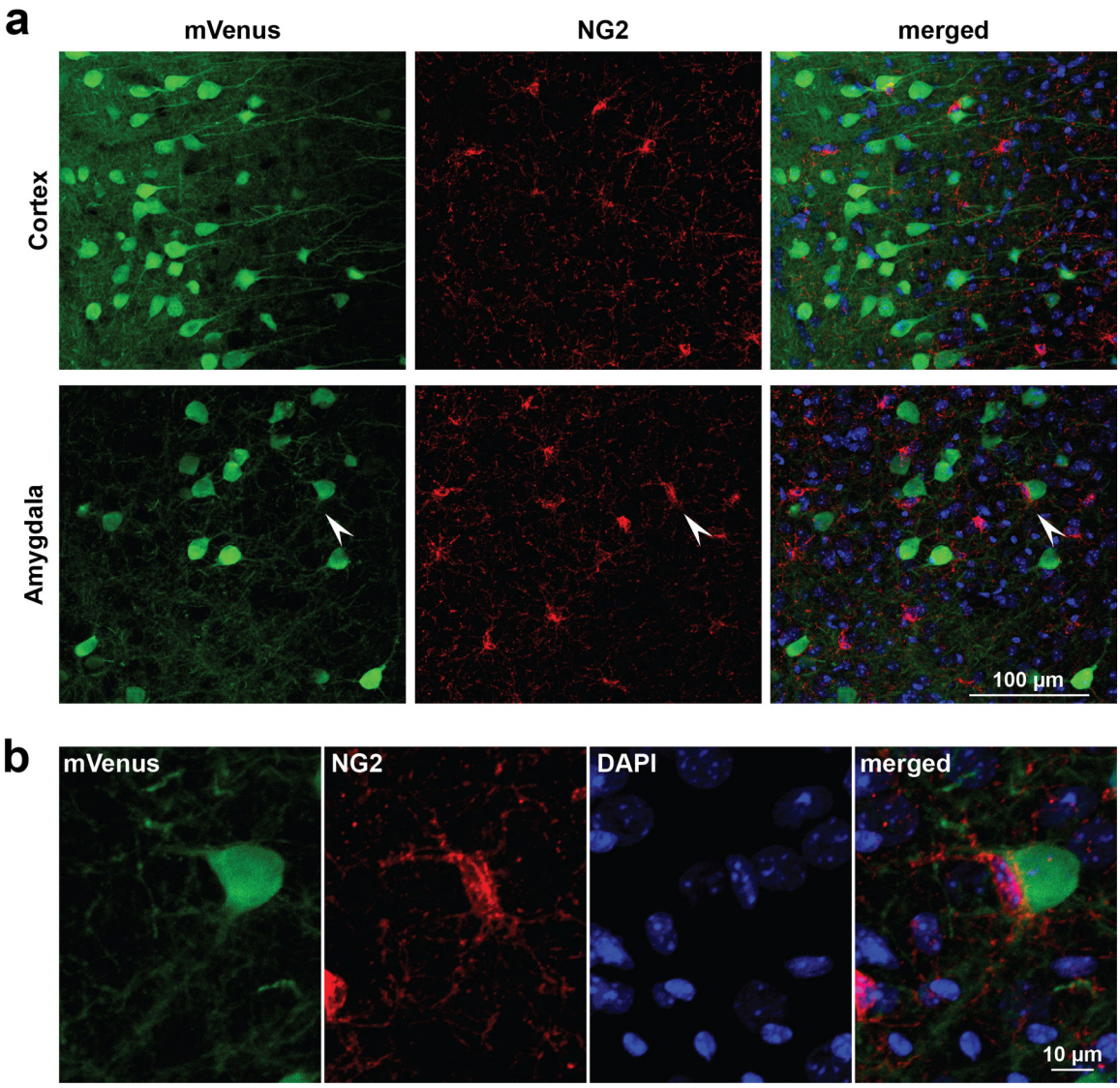

Extended Data Figure 5.

(**a**) NG2 (Neuron-glial antigen 2) expression in brain sections from mice infected with YFV-mVenus. NG2 is a marker of NG2 cells (also referred to as oligodendrocyte precursor cells). The green fluorescence was from native mVenus without immunostaining. (**b**) High-resolution images of the areas indicated by arrowheads in **a**, showing a NG2-positive cell next to a mVenus-positive cell. (n=25 brain sections from 3 mice). The images are tile scans of brain sections. The blue color is counterstaining with DAPI.

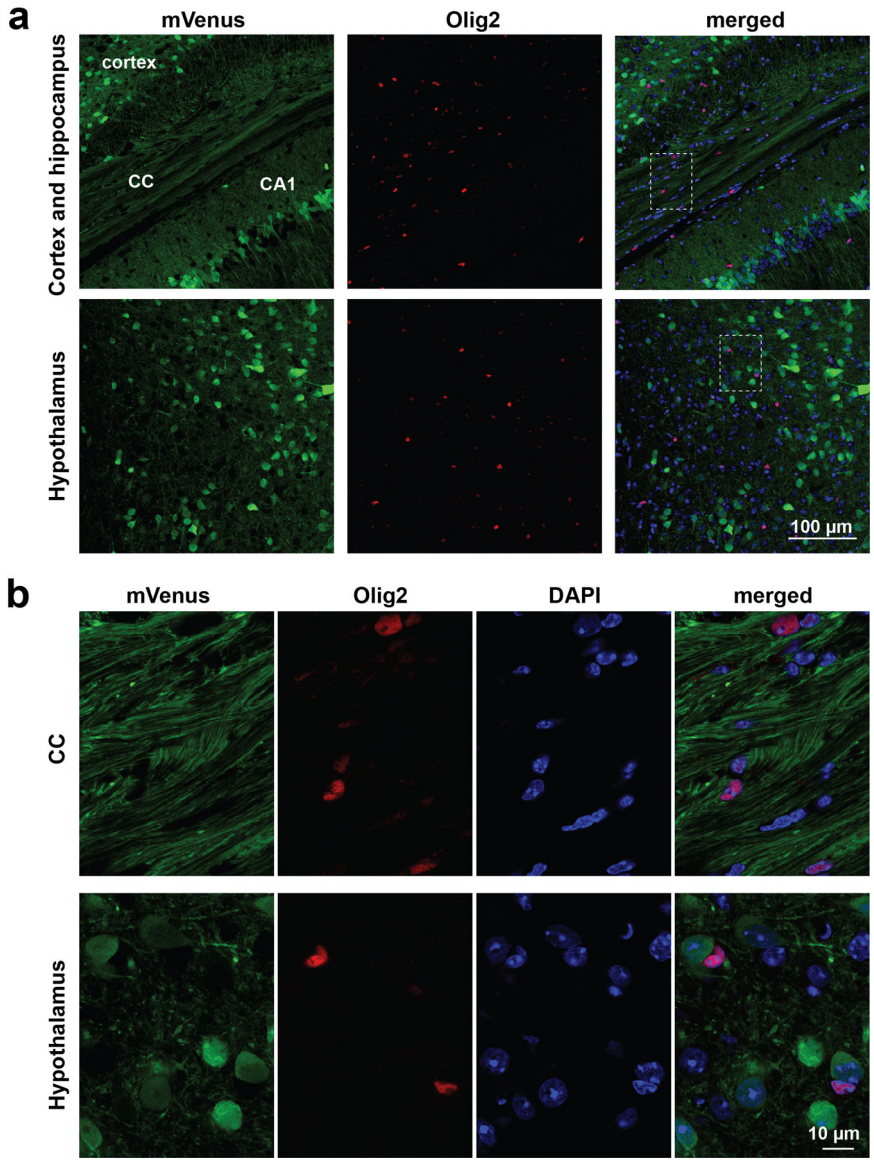

Extended Data Figure 6.

(**a**) Olig2 (a marker of oligodendrocytes) expression in brain sections from mice infected with YFV-mVenus. The green fluorescence was from native mVenus without immunostaining. (**b**) High-resolution images of the cropped areas in **a**. CC: corpus callosum. n=26 brain sections from 3 mice. The images are tile scans of brain sections. The blue color is counterstaining with DAPI.

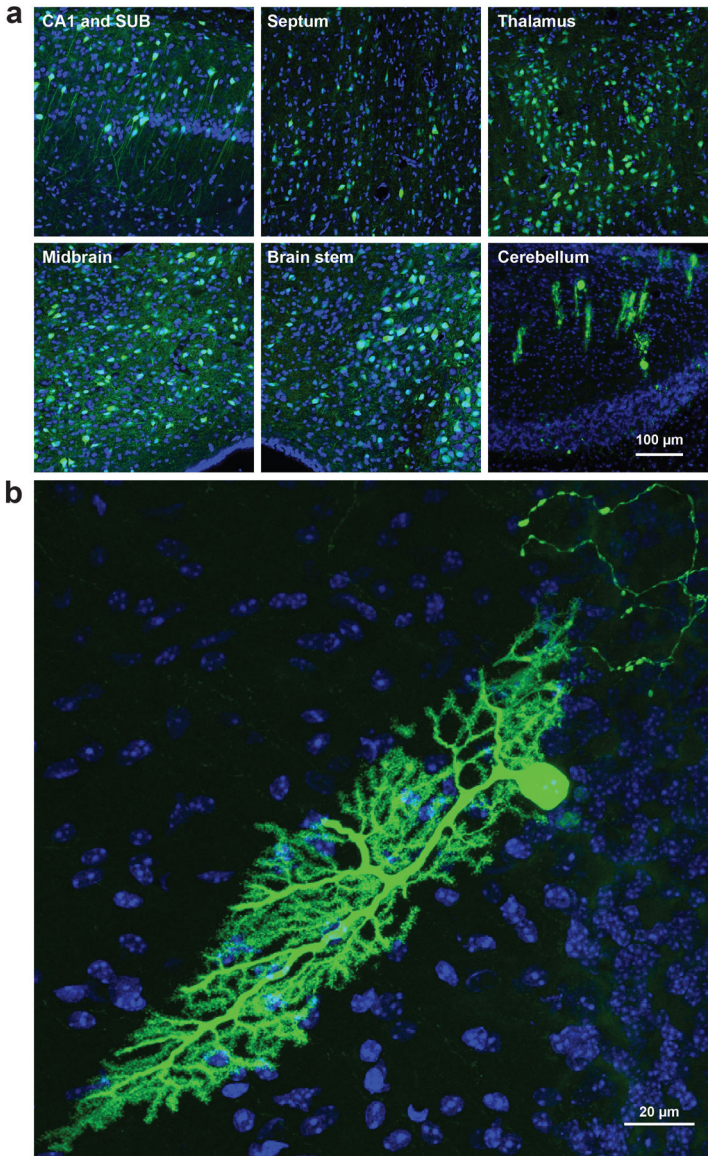

Extended Data Figure 7.

(**a**) Expression of mVenus in multiple brain regions after injection of YFV-mVenus into the PFC and fixation of the brains 15 days later. (**b**) Expression of mVenus in a cerebellar Purkinje cell. The experiments were repeated 6 times with similar results. The images are tile scans of brain sections. The blue color is counterstaining with DAPI.

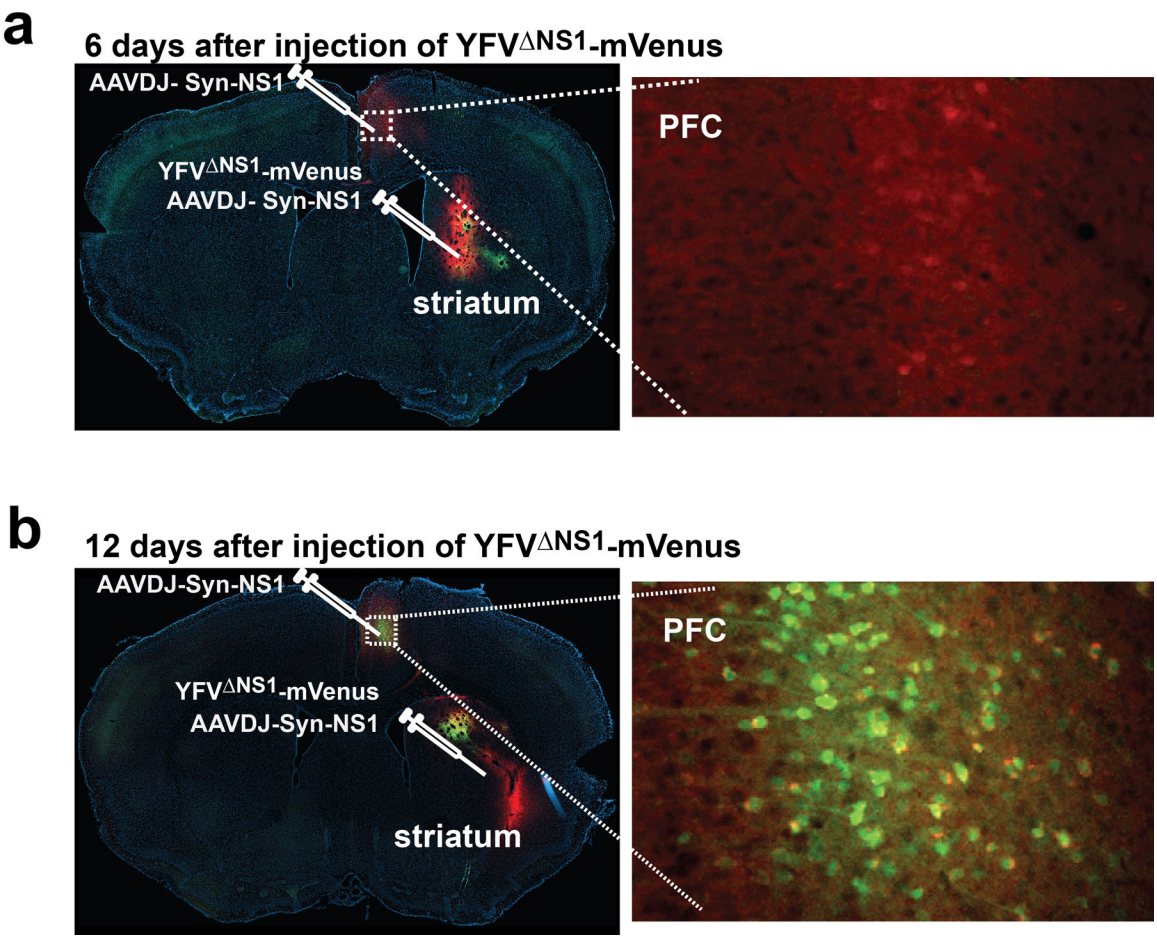

Extended Data Figure 8.

Expression of mVenus and tdTomato after Injection of AAVDJ-Syn-NS1 into the PFC and the striatum, and injection of YFV$^{\Delta NS1}$-mVenus into the striatum. The brains were fixed 6 (**a**) or 12 (**b**) days after YFV$^{\Delta NS1}$-mVenus injection. The experiments were repeated 3 times with similar results. The images are tile scans of brain sections. The blue color is counterstaining with DAPI.

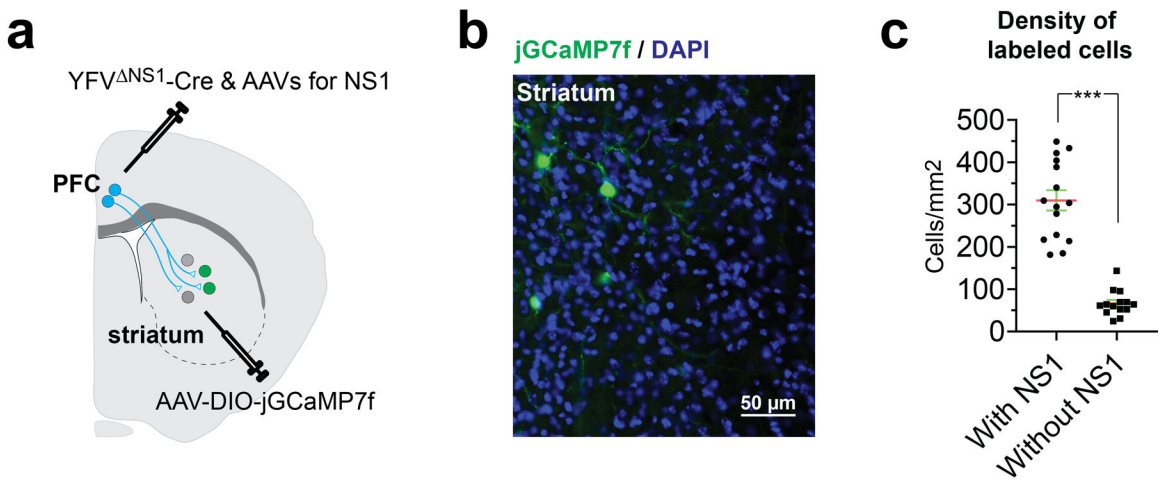

Extended Data Figure 9.

(**a**) The experimental design was the same as in Fig. 4b–d except that no AAVs for NS1 expression were injected into the striatum. We fixed the brains 15 days after YFV$^{\Delta NS1}$-Cre injections. (**b**) jGCaMP7f-positive neurons in the striatum. The image is a tile scan of the brain section. The blue color is counterstaining with DAPI. (**c**) The density of labeled cells in mice with or without NS1 in the striatum (n=15 sections from 4 mice for “with NS1” and n=14 sections from 4 mice “without NS1”, *** P=0.000000026, Mann-Whitney test, two tailed). The data of the group “with NS1” were also shown in Fig. 4d.

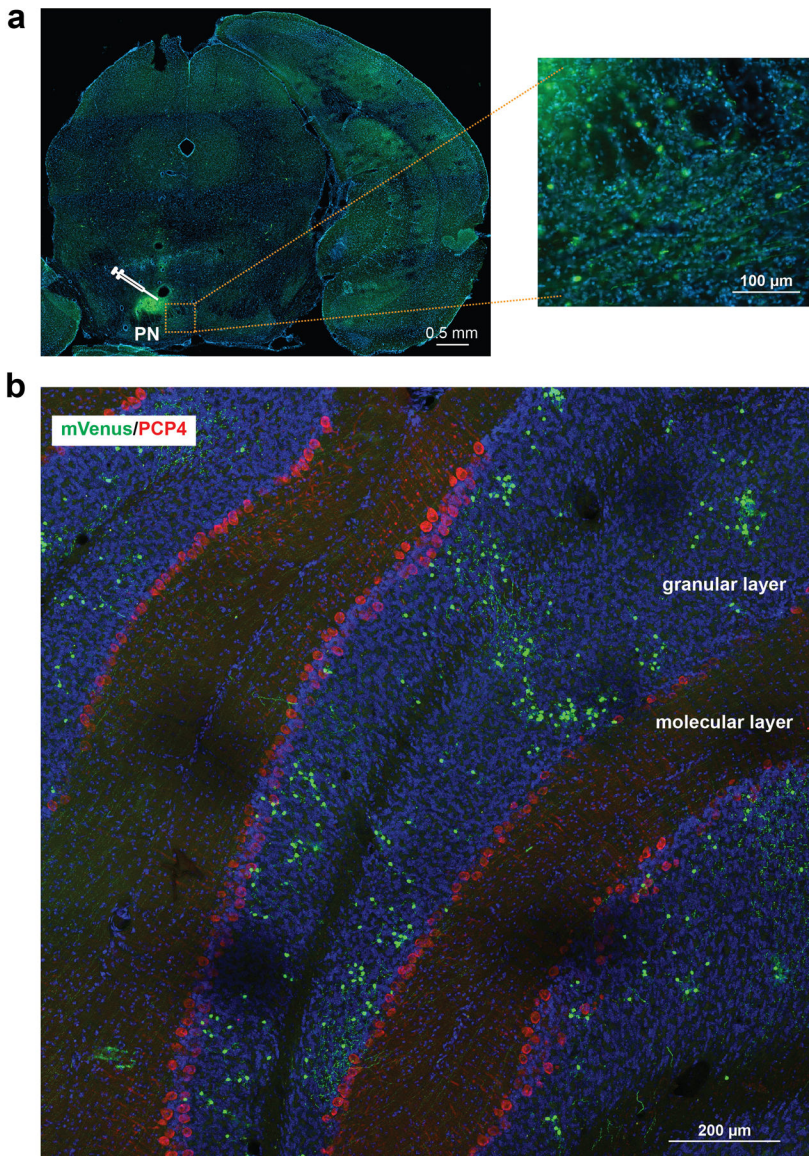

Extended Data Figure 10.

(**a**) Image of a brain section after injection of AAV-tTA, AAV-TRE-C-prM-E-NS1 and YFV$^{\Delta CME}$-mVenus into pontine nucleus and adjacent reticular tegmental nucleus. (**b**) mVenus-positive cells in the granular layer of the cerebellar cortex. The sections were counterstained with a marker for Purkinje cells, PCP4 (red), and DAPI (Blue). The experiments were repeated 4 times with similar results. The images are tile scans of brain sections. The blue color is counterstaining with DAPI.

Supplementary Material

Refer to Web version on PubMed Central for supplementary material.

Acknowledgments

We thank Dr. Ege Kavalali for critical comments and suggestions. This study was supported by Klingenstein-Simons Fellowship Awards in Neuroscience (to WX) and grants NIH/NINDS (NS104828 to WX), NIH/NIMH (MH099153 to WX), and NIH/NIAID (AI117922 to JS). UT BRAIN seed grants (365231) and Texas Institute for Brain Injury and Repair (TIBIR) pilot grant provided funds to initiate this study. We thank Dr. Denise Ramirez, Dr. Julian Meeks and the Whole Brain Microscopy Facility at UT Southwestern; and Dr. Shin Yamazaki (Neuroscience Microscopy Facility at UT Southwestern) for help with imaging.

Data Availability Statement:

The original data in this study include images of brain sections, calcium imaging data of freely moving mice and sequences of plasmids. The sequences of the plasmids have been deposited to Genbank as follows: pAAV-DIO-NS1 (MZ708030), pAAV-Syn-NS1-p2A-NLSdTomato (MZ695807), pAAV-rtTA (MZ708018), pAAV-SynaptoTAG2 (MZ708019), pAAV-TRE-C-prM-E-NS1 (MZ708020), pAAV-TRE-NS1-dTomato (MZ708021), pAAV-TRE-NS1NF (MZ708022), pAAV-tTA (MZ708023), pFUW-C-prM-E-NS1 (MZ708024), pYFVdelCME-mVenus (MZ708025), pYFVdeltaCMENS1-Cre (MZ708026), pYFVdeltaNS1-Cre (MZ708027), pYFVdeltaNS1-mCherry (MZ708028), and pYFVdeltaNS1-mVenus (MZ708029). The plasmids have been deposited to Addgene as follows: pAAV-DIO-NS1 (plasmid 175273), pAAV-Syn-NS1-p2A-NLSdTomato (plasmid 175276), pAAV-rtTA (plasmid 175274), pAAV-SynaptoTAG2 (plasmid 175275), pAAV-TRE-C-prM-E-NS1 (plasmid 175277), pAAV-TRE-NS1-dTomato (plasmid 175278), pAAV-TRE-NS1NF (plasmid 175279), pAAV-tTA (plasmid 175280), and pFUW-C-prM-E-NS1 (plasmid 175281). The other plasmids or reagents can be requested from the corresponding authors. The raw imaging data are of large file sizes (totally >100 GB) and can be requested from the corresponding authors.

References

1. Zeng H & Sanes JR Neuronal cell-type classification: challenges, opportunities and the path forward. Nat Rev Neurosci 18, 530–546 (2017). [PubMed: 28775344]
2. Callaway EM Transneuronal circuit tracing with neurotropic viruses. Curr Opin Neurobiol 18, 617–623 (2008). [PubMed: 19349161]
3. Ekstrand MI, Enquist LW & Pomeranz LE The alpha-herpesviruses: molecular pathfinders in nervous system circuits. Trends Mol Med 14, 134–140 (2008). [PubMed: 18280208]
4. Miyamichi K et al. Cortical representations of olfactory input by trans-synaptic tracing. Nature 472, 191–196 (2011). [PubMed: 21179085]
5. Oyibo HK, Znamenskiy P, Oviedo HV, Enquist LW & Zador AM Long-term Cre-mediated retrograde tagging of neurons using a novel recombinant pseudorabies virus. Front Neuroanat 8, 86 (2014). [PubMed: 25232307]
6. Wickersham IR et al. Monosynaptic restriction of transsynaptic tracing from single, genetically targeted neurons. Neuron 53, 639–647 (2007). [PubMed: 17329205]
7. Osakada F et al. New rabies virus variants for monitoring and manipulating activity and gene expression in defined neural circuits. Neuron 71, 617–631 (2011). [PubMed: 21867879]
8. Enquist LW Exploiting circuit-specific spread of pseudorabies virus in the central nervous system: insights to pathogenesis and circuit tracers. J Infect Dis 186 Suppl 2, S209–214 (2002). [PubMed: 12424699]
9. Wojaczynski GJ, Engel EA, Steren KE, Enquist LW & Patrick Card J The neuroinvasive profiles of H129 (herpes simplex virus type 1) recombinants with putative anterograde-only transneuronal spread properties. Brain Struct Funct 220, 1395–1420 (2015). [PubMed: 24585022]

10. Zemanick MC, Strick PL & Dix RD Direction of transneuronal transport of herpes simplex virus 1 in the primate motor system is strain-dependent. Proc Natl Acad Sci U S A 88, 8048–8051 (1991). [PubMed: 1654557]
11. Lo L & Anderson DJ A Cre-dependent, anterograde transsynaptic viral tracer for mapping output pathways of genetically marked neurons. Neuron 72, 938–950 (2011). [PubMed: 22196330]
12. Zeng WB et al. Anterograde monosynaptic transneuronal tracers derived from herpes simplex virus 1 strain H129. Mol Neurodegener 12, 38 (2017). [PubMed: 28499404]
13. Dix RD, McKendall RR & Baringer JR Comparative neurovirulence of herpes simplex virus type 1 strains after peripheral or intracerebral inoculation of BALB/c mice. Infect Immun 40, 103–112 (1983). [PubMed: 6299955]
14. Itzhaki RF Corroboration of a Major Role for Herpes Simplex Virus Type 1 in Alzheimer's Disease. Front Aging Neurosci 10, 324 (2018). [PubMed: 30405395]
15. Beier KT et al. Anterograde or retrograde transsynaptic labeling of CNS neurons with vesicular stomatitis virus vectors. Proc Natl Acad Sci U S A 108, 15414–15419 (2011). [PubMed: 21825165]
16. Zingg B et al. AAV-Mediated Anterograde Transsynaptic Tagging: Mapping Corticocollicular Input-Defined Neural Pathways for Defense Behaviors. Neuron 93, 33–47 (2017). [PubMed: 27989459]
17. Castle MJ, Gershenson ZT, Giles AR, Holzbaur EL & Wolfe JH Adeno-associated virus serotypes 1, 8, and 9 share conserved mechanisms for anterograde and retrograde axonal transport. Hum Gene Ther 25, 705–720 (2014). [PubMed: 24694006]
18. Burger C et al. Recombinant AAV viral vectors pseudotyped with viral capsids from serotypes 1, 2, and 5 display differential efficiency and cell tropism after delivery to different regions of the central nervous system. Mol Ther 10, 302–317 (2004). [PubMed: 15294177]
19. Mukhopadhyay S, Kuhn RJ & Rossmann MG A structural perspective of the flavivirus life cycle. Nat Rev Microbiol 3, 13–22 (2005). [PubMed: 15608696]
20. Yi Z et al. Identification and characterization of the host protein DNAJC14 as a broadly active flavivirus replication modulator. PLoS Pathog 7, e1001255 (2011). [PubMed: 21249176]
21. Voorn P, Vanderschuren LJ, Groenewegen HJ, Robbins TW & Pennartz CM Putting a spin on the dorsal-ventral divide of the striatum. Trends Neurosci 27, 468–474 (2004). [PubMed: 15271494]
22. Bienkowski MS et al. Integration of gene expression and brain-wide connectivity reveals the multiscale organization of mouse hippocampal networks. Nat Neurosci 21, 1628–1643 (2018). [PubMed: 30297807]
23. Tervo DG et al. A Designer AAV Variant Permits Efficient Retrograde Access to Projection Neurons. Neuron 92, 372–382 (2016). [PubMed: 27720486]
24. Lindenbach BD & Rice CM trans-Complementation of yellow fever virus NS1 reveals a role in early RNA replication. J Virol 71, 9608–9617 (1997). [PubMed: 9371625]
25. Dana H et al. High-performance calcium sensors for imaging activity in neuronal populations and microcompartments. Nat Methods 16, 649–657 (2019). [PubMed: 31209382]
26. Boudkkazi S et al. Release-dependent variations in synaptic latency: a putative code for short- and long-term synaptic dynamics. Neuron 56, 1048–1060 (2007). [PubMed: 18093526]
27. Barbera G et al. Spatially Compact Neural Clusters in the Dorsal Striatum Encode Locomotion Relevant Information. Neuron 92, 202–213 (2016). [PubMed: 27667003]
28. Xu W & Sudhof TC A neural circuit for memory specificity and generalization. Science 339, 1290–1295 (2013). [PubMed: 23493706]
29. van Strien NM, Cappaert NL & Witter MP The anatomy of memory: an interactive overview of the parahippocampal-hippocampal network. Nat Rev Neurosci 10, 272–282 (2009). [PubMed: 19300446]
30. Reardon TR et al. Rabies Virus CVS-N2c(DeltaG) Strain Enhances Retrograde Synaptic Transfer and Neuronal Viability. Neuron 89, 711–724 (2016). [PubMed: 26804990]
31. Chatterjee S et al. Nontoxic, double-deletion-mutant rabies viral vectors for retrograde targeting of projection neurons. Nat Neurosci 21, 638–646 (2018). [PubMed: 29507411]

32. Ciabatti E, Gonzalez-Rueda A, Mariotti L, Morgese F & Tripodi M Life-Long Genetic and Functional Access to Neural Circuits Using Self-Inactivating Rabies Virus. Cell 170, 382–392 e314 (2017). [PubMed: 28689641]
33. Gradinaru V et al. Molecular and cellular approaches for diversifying and extending optogenetics. Cell 141, 154–165 (2010). [PubMed: 20303157]
34. Libbrecht S, Van den Haute C, Malinouskaya L, Gijsbers R & Baekelandt V Evaluation of WGA-Cre-dependent topological transgene expression in the rodent brain. Brain Struct Funct 222, 717–733 (2017). [PubMed: 27259586]
35. Inagaki HK et al. Visualizing neuromodulation in vivo: TANGO-mapping of dopamine signaling reveals appetite control of sugar sensing. Cell 148, 583–595 (2012). [PubMed: 22304923]
36. Jagadish S, Barnea G, Clandinin TR & Axel R Identifying functional connections of the inner photoreceptors in Drosophila using Tango-Trace. Neuron 83, 630–644 (2014). [PubMed: 25043419]
37. Huang TH et al. Tracing neuronal circuits in transgenic animals by transneuronal control of transcription (TRACT). Elife 6, doi:10.7554/eLife.32027 (2017).
38. Barrett ADT Yellow fever live attenuated vaccine: A very successful live attenuated vaccine but still we have problems controlling the disease. Vaccine 35, 5951–5955 (2017). [PubMed: 28366605]
39. Yi Z et al. Identification and characterization of the host protein DNAJC14 as a broadly active flavivirus replication modulator. PLoS Pathog 7, e1001255, doi:10.1371/journal.ppat.1001255 (2011). [PubMed: 21249176]
40. Zolotukhin S et al. Recombinant adeno-associated virus purification using novel methods improves infectious titer and yield. Gene Ther 6, 973–985 (1999). [PubMed: 10455399]
41. Barbera G et al. Spatially Compact Neural Clusters in the Dorsal Striatum Encode Locomotion Relevant Information. Neuron 92, 202–213 (2016). [PubMed: 27667003]
42. Pnevmatikakis EA & Giovannucci A NoRMCorre: An online algorithm for piecewise rigid motion correction of calcium imaging data. J Neurosci Methods 291, 83–94 (2017). [PubMed: 28782629]
43. Zhou P et al. Efficient and accurate extraction of in vivo calcium signals from microendoscopic video data. Elife 7, doi:10.7554/eLife.28728 (2018).

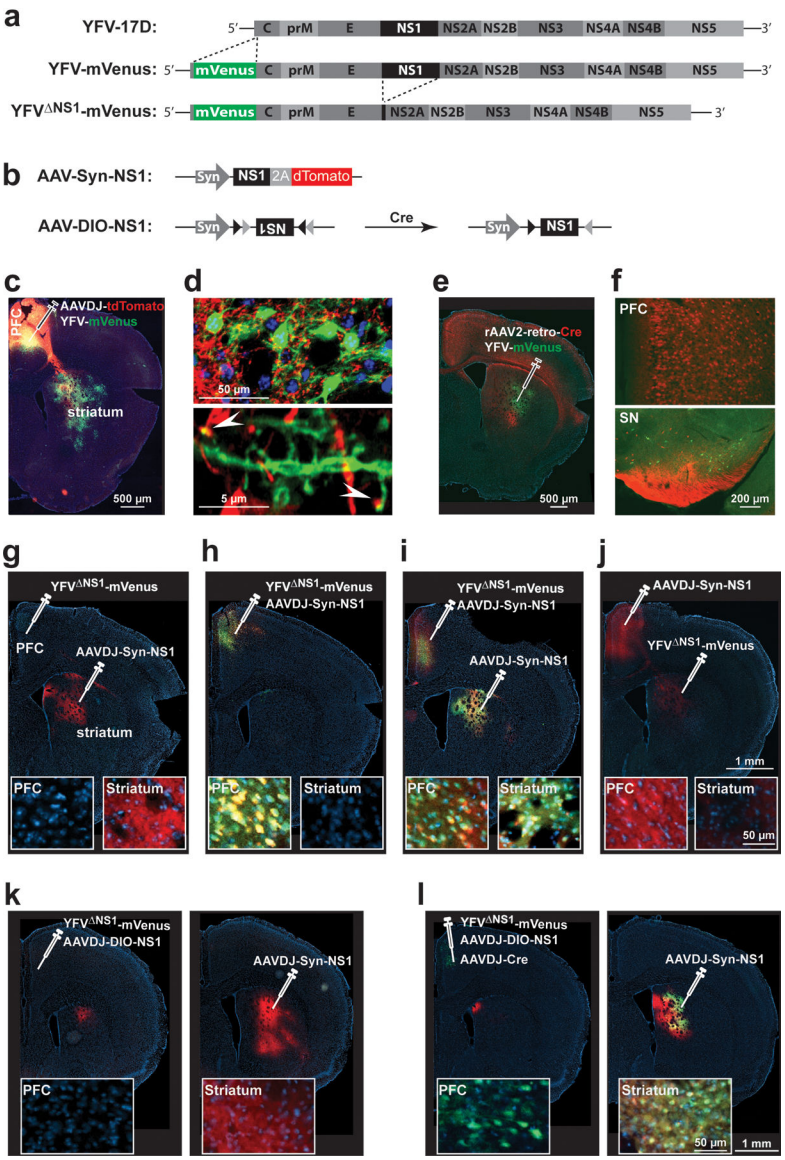

Figure 1. Controlled anterograde transneuronal spreading of YFV-17D.

(**a**) Construction of YFV-mVenus and YFV$^{\Delta NS1}$-mVenus. (**b**) AAVs mediating constitutive (AAV-Syn-NS1) or conditional (AAV-DIO-NS1) expression of NS1. (**c**, **d**) Expression of mVenus and tdTomato after injection of YFV-mVenus and AAVDJ-tdTomato into the PFC. (**d**) Top: mVenus-positive neurons and tdTomato-positive axons in the striatum. Bottom: contacts between mVenus-positive neurons and tdTomato-positive axonal terminals are indicated by arrowheads. (**e, f**) Expression of mVenus and tdTomato (representing Cre) after injection of YFV-mVenus and rAAV2-retro-Cre into the striatum of an Ai9 mouse. (**f**) mVenus and tdTomato (representing Cre) in the PFC (top) and SN (bottom). (**g**) Expression of NS1 after injection of AAVDJ-Syn-NS1 and YFV$^{\Delta NS1}$-mVenus into the striatum and the PFC, respectively. (**h**) Expression of NS1 and mVenus after injection of AAVDJ-Syn-NS1 and YFV$^{\Delta NS1}$-mVenus into the PFC. (**i**) Expression of NS1 and mVenus after injection of AAVDJ-Syn-NS1 into the PFC and striatum, and YFV$^{\Delta NS1}$-mVenus into the PFC. (**j**)

Expression of NS1 after injection of AAVDJ-Syn-NS1 into the PFC and YFV$^{\Delta NS1}$-mVenus into the striatum. (**k**) Expression of NS1 after injection of AAVDJ-DIO-NS1 and YFV$^{\Delta NS1}$-mVenus into the PFC, and AAVDJ-NS1 into the striatum. (**l**) Expression of NS1 and mVenus after injection of AAVDJ-DIO-NS1, AAV-Cre and YFV$^{\Delta NS1}$-mVenus into the PFC, and AAVDJ-NS1 into the striatum. All images except Fig. 1d are tile scans of brain sections. The blue color is counterstaining with DAPI. The experiments in Fig. 1c–d, e–f, g, j, k and l were repeated 3 times with similar results. The experiments in Fig. 1h and iv were repeated 4 times with similar results.

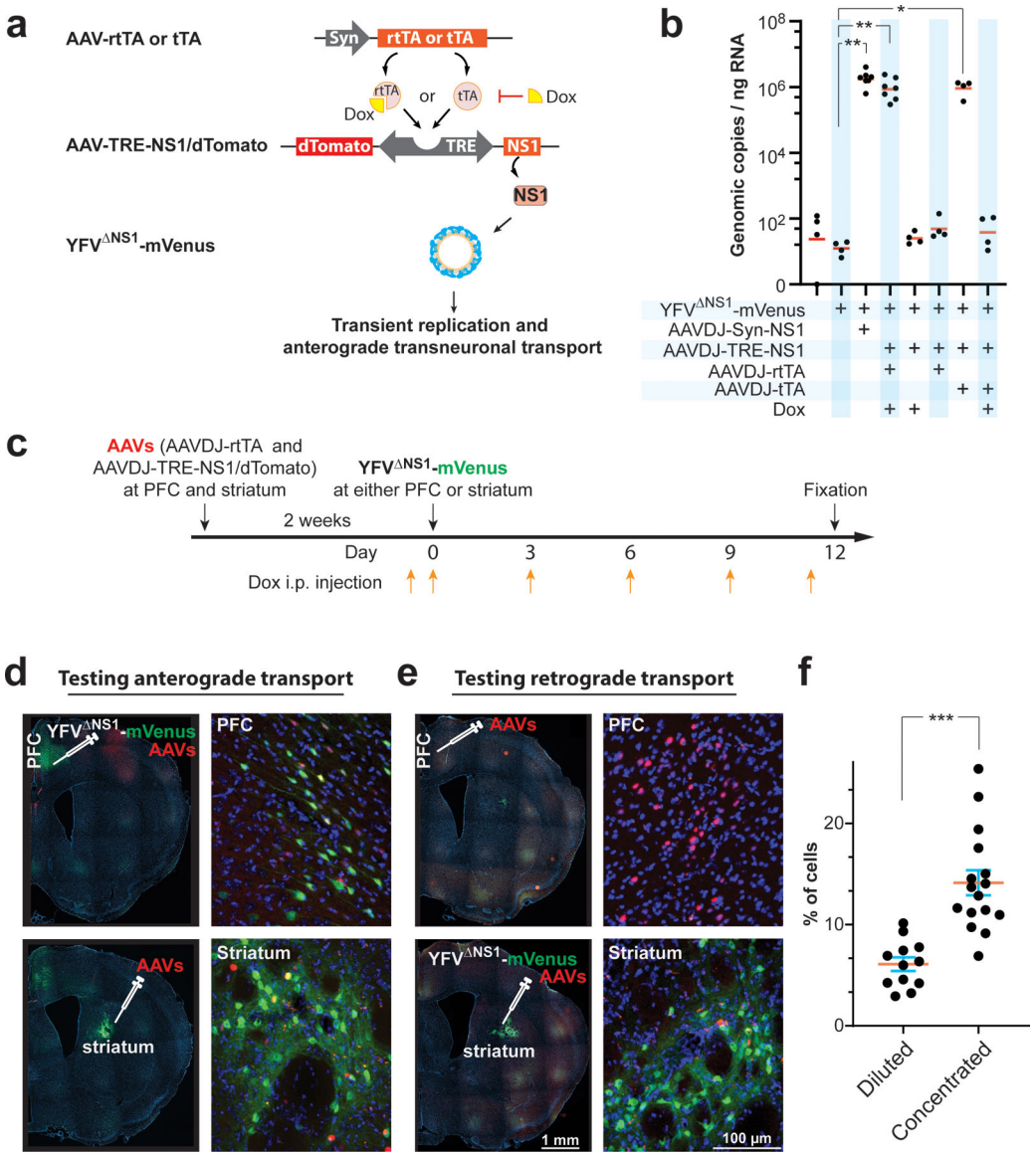

Figure 2. Anterograde-only tracing by inducible replication of YFV$^{\Delta NS1}$.

(**a**) Schematics showing viral vectors mediating inducible expression of NS1 and replication of YFV$^{\Delta NS1}$-mVenus. (**b**) Quantification of the genomic copies of YFV$^{\Delta NS1}$-mVenus in PFC after injection of the indicated AAVs and YFV$^{\Delta NS1}$-mVenus into the PFC. Data are presented as scatter and mean. n=4–7 mice in each group, * *P*=0.029, ** *P=0.0061*, Mann-Whitney test, two tailed, compared to mice receiving YFV$^{\Delta NS1}$-mVenus alone. (**c**) Experimental procedures for **d** and **e**. (**d**) Expression of tdTomato and mVenus after injection of AAVDJ-rtTA and AAVDJ-TRE-NS1/dTomato into both the PFC and the striatum and YFV$^{\Delta NS1}$-mVenus into the PFC. (**e**) Expression of tdTomato and mVenus after injection of AAVDJ-rtTA and AAVDJ-TRE-NS1/dTomato into both the PFC and the striatum, YFV$^{\Delta NS1}$-mVenus into the striatum. The images in **d-e** are tile scans of brain sections. The blue color is counterstaining with DAPI. (**f**) Percentage of mVenus-positive cells after the mice underwent the same procedure as in **d** with either concentrated or 5 to 10-fold

diluted YFV$^{\Delta NS1}$-mVenus injected into the PFC. We counted mVenus-positive cells and DAPI-stained nuclei in the striatum to calculate the tracing efficiency. Data are presented as scatter and mean±standard error of the mean (SEM), n=12 and 16 brain sections from 4 mice per group for “diluted” and “concentrated”, respectively. *** P=0.000004, Mann-Whitney test, two tailed. The experiments in Fig. 2d and e were repeated 4 times with similar results.

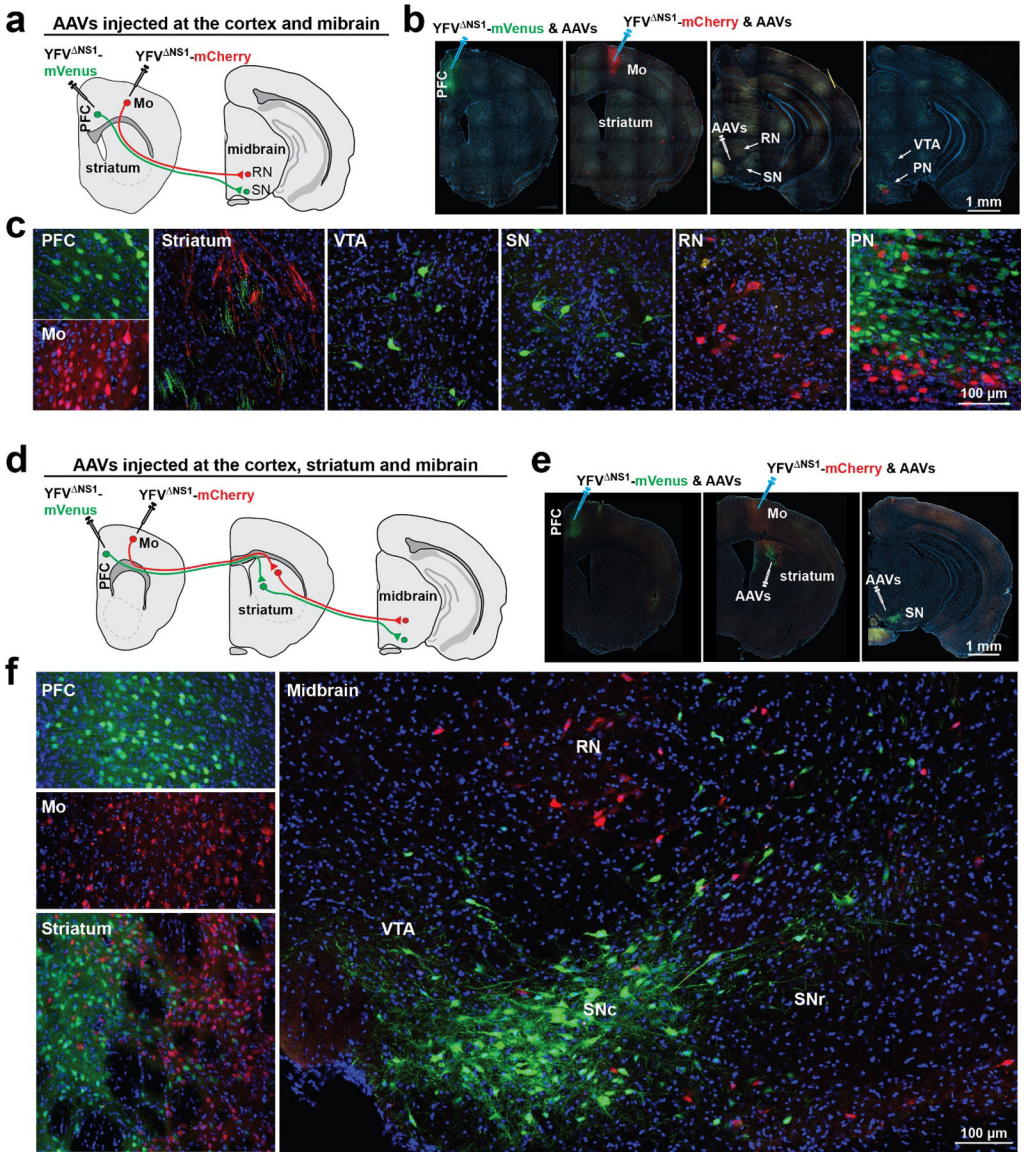

Figure 3. Dual fluorescence tracing of parallel circuits.

(**a-c**) Tracing long-range projections from the cortical regions to the midbrain with YFV$^{\Delta NS1}$. (**a**) Schematics showing the neuronal pathways and viral injections. The AAVs include AAVDJ-rtTA and AAVDJ-TRE-NS1. (**b, c**) Representative images showing mVenus- or mCherry- positive neurons or axons in the cortex, striatum and midbrain nuclei. (**d-f**) Tracing polysynaptic projections from the cortical regions via the striatum to the midbrain with YFV$^{\Delta NS1}$. (**d**) The mice received the same viral injections as those in **a** except that the AAVs were also injected into the striatum. (**e, f**) Representative images showing mVenus- or mCherry- positive neurons in the cortex, striatum and midbrain nuclei. All images are tile scans of brain sections. The blue color is counterstaining with DAPI. The experiments in Fig. 3a–c, Fig. 3d–f were repeated 3 times with similar results.

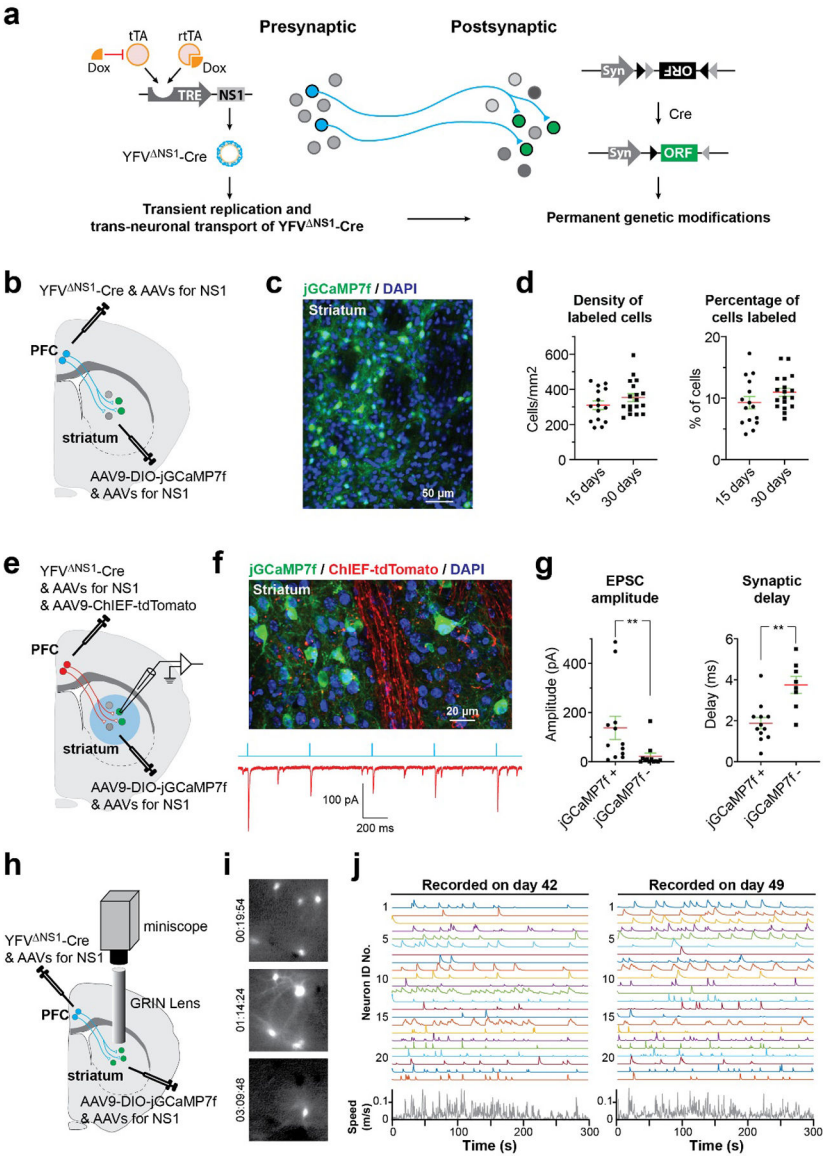

Figure 4. Transneuronal genetic control by YFV$^{\Delta NS1}$-Cre.

(**a**) Schematic of transneuronal genetic modification with YFV$^{\Delta NS1}$-Cre. (**b-d**) Injection of YFV$^{\Delta NS1}$-Cre into PFC to turn on a reporter in the striatum. (**b**) Viral injection scheme. Brains were fixed 15 or 30 days after YFV$^{\Delta NS1}$-Cre injection. (**c**) Expression of jGCaMP7f in the striatum. (**d**) Quantification of the densities (left) or percentage (right) of jGCaMP7f-labeled striatal neurons. Data are presented as scatter and mean±SEM, n=15–18 brain sections from 4 mice per group. *P*=0.26 for “Density” and *P*=0.13 for “Percentage”, Mann-Whitney test, two tailed. (**e-g**) Electrophysiological recording of striatal neurons with optogenetic stimulation of axons from the PFC. (**e**) Viral injection scheme. (**f**) Top: jGCaMP7f-positive striatal neurons and tdTomato-positive axons. Bottom: a representative trace of postsynaptic currents. The blue bars indicate optogenetic stimulation. (**g**) The amplitudes (n=12 cells from 3 mice, left) and synaptic delays (n=12 and 8 cells for jGCaMP7f- positive and -negative cells, respectively, right) of synaptic currents. Data are

presented as scatter and mean±SEM ** P=0.0011 for “EPSC amplitude” and P=0.0019 for “Synaptic delay”, Mann-Whitney test, two tailed. (**h**-**j**) Imaging neuronal calcium activities in freely moving mice. (**h**) Viral injections and lens implantation. (**i**) Individual image frames. (**j**) Neuronal calcium activities of a mouse recorded on day 42 and day 49 after $YFV^{\Delta NS1}$-Cre injection, respectively. Calcium activity (ΔF/F) of individual neurons was plotted together with the locomotion speed of the mouse. Images in 4**c** and **f** are tile scans of brain sections. The blue color is counterstaining with DAPI. The experiments in Fig. 4h–j were repeated 3 times with similar results.

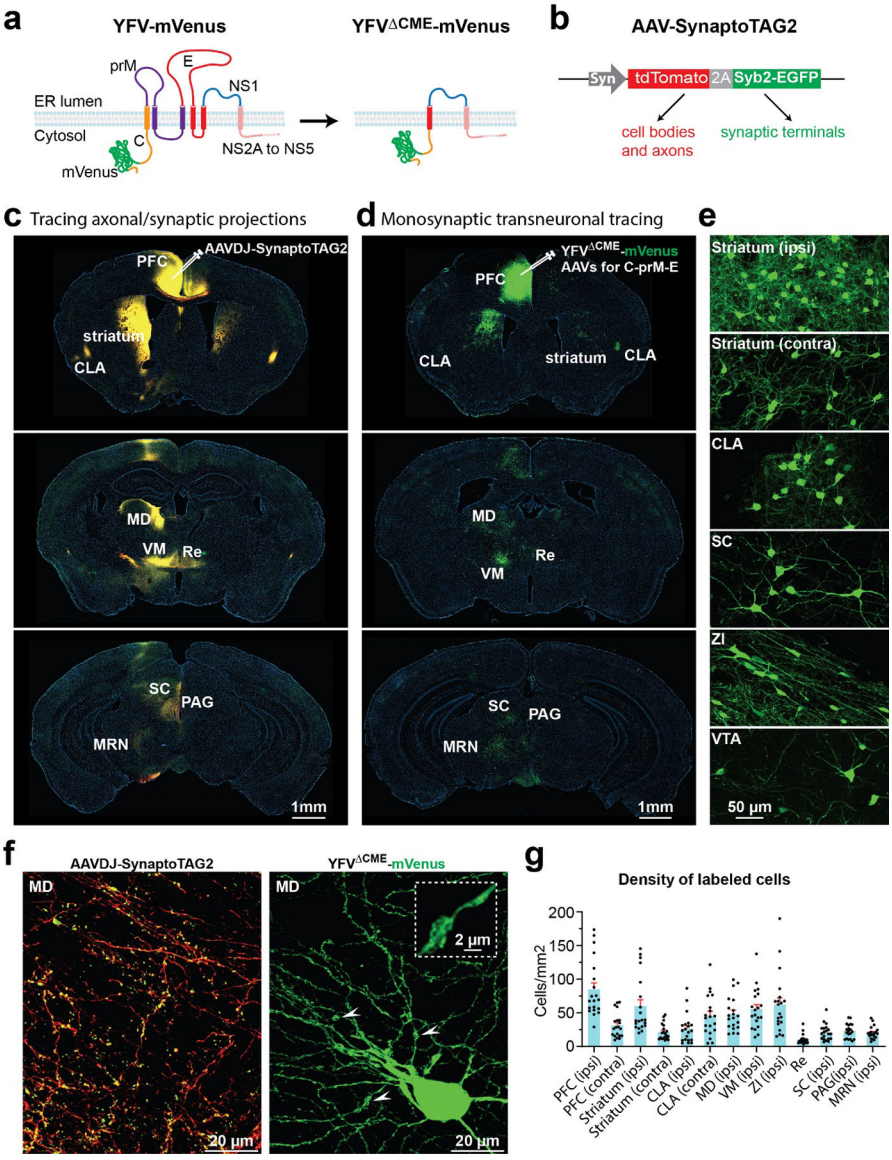

Figure 5. Mapping monosynaptic projectomes with YFV$^{\Delta CME}$.

(**a**) Construction of YFV$^{\Delta CME}$-mVenus by removing the coding sequences of three structural proteins (C-prM-E). (**b**) Mapping axonal and synaptic projections of neurons with AAV-SynaptoTAG2. (**c**) Distribution of tdTomato and Syb2-EGFP after injection of AAVDJ-SynaptoTAG2 into the PFC. (**d, e**) Distribution of mVenus after injection of YFV$^{\Delta CME}$-mVenus, AAVDJ-tTA and AAVDJ-C-prM-E-NS1 into the PFC. Abbreviations: CLA, claustrum; MD, mediodorsal nucleus of the thalamus; VM, ventromedial thalamic nucleus; Re, nucleus reuniens; ZI, zona incerta; SC, superior colliculus; MRN, midbrain reticular nucleus; PAG, periaqueductal grey area. (**f**) Left: Axons (red) and synaptic terminals (green) labeled by SynaptoTAG2. Right: Postsynaptic neurons traced by YFV$^{\Delta CME}$-mVenus. The arrowheads and insert show the mossy tuft-like structures on the dendrite. (**g**) Quantification of the density of neurons traced by YFV$^{\Delta CME}$-mVenus. Data are presented as scatter and mean+SEM, n=20 brain sections from 4 mice for each region. Ipsi and contra: ipsilateral or

contralateral to the injection site. Images in **c** and **d** are tile scans of brain sections. The blue color is counterstaining with DAPI. The experiments in Fig. 5c–f were repeated 4 times with similar results.

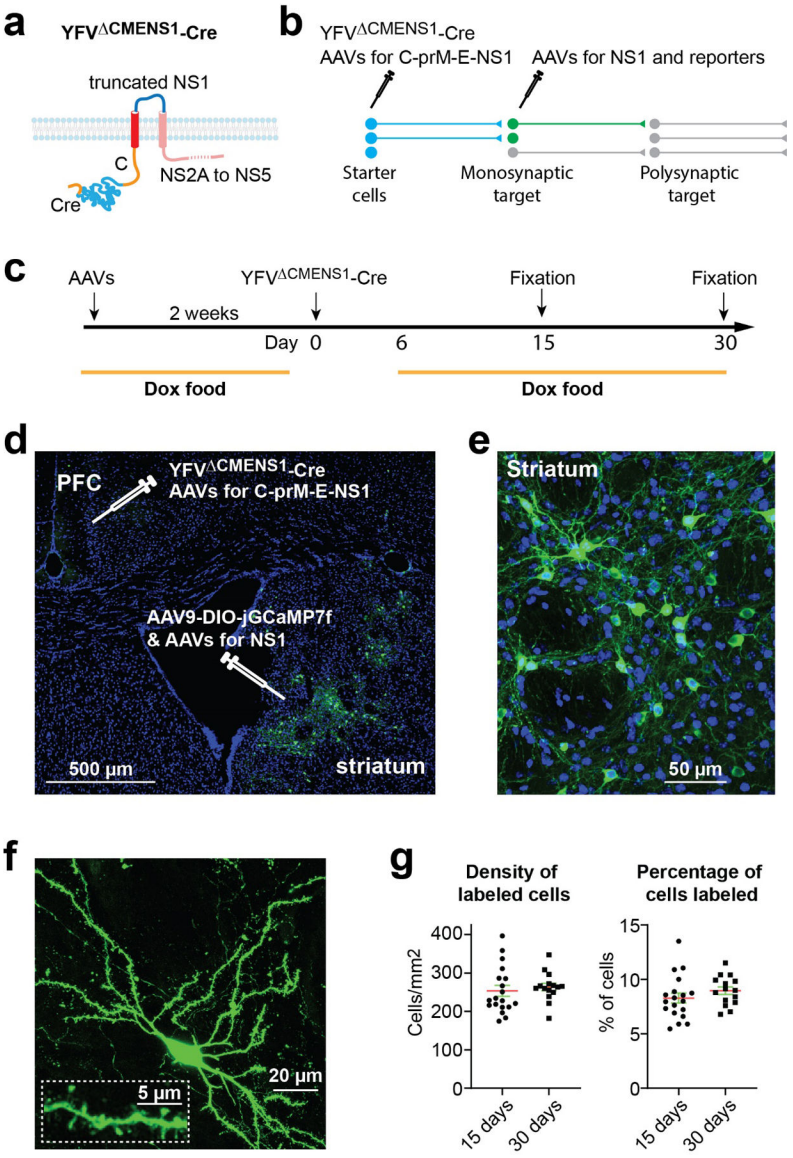

Figure 6. Monosynaptic transneuronal genetic control with YFV$^{\Delta CMENS1}$.

(**a**) Construction of YFV$^{\Delta CMENS1}$-Cre by removing the coding sequences of C-prM-E and NS1. (**b**) Schematic showing monosynaptic transneuronal genetic control with YFV$^{\Delta CMENS1}$-Cre. (**c**) The scheme of viral injections and Dox diet. The AAVs include AAVDJ-tTA and AAVDJ-TRE-C-prM-E-NS1 or AAVDJ-TRE-NS1. (**d-g**) Injection of YFV$^{\Delta CMENS1}$–Cre into the PFC to turn on the reporter in the striatum. (**d**) jGCaMP7f expression after injection of AAVDJ-tTA, AAVDJ-TRE-C-prM-E-NS1 and YFV$^{\Delta CMENS1}$–Cre into the PFC and AAVDJ-tTA, AAVDJ-TRE-NS1 and AAV9-DIO-jGCaMP into the striatum. (**e**) jGCaMP7f-positve neurons in the striatum. (**f**) Expression of jGCaMP7f in striatal neurons. The insert shows the spines on a segment of a dendrite. (**g**) Quantification of the traced neurons in the striatum. Data are presented as scatter and mean±SEM, n=15–19 brain sections from 3–4 mice. *P*=0.26 for “density” and 0.16 for “percentage”, Mann-

Whitney test, two tailed. Images in 6**d**-**e** are tile scans of brain sections. The blue color is counterstaining with DAPI.